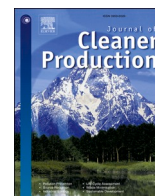# bradscholars

A comprehensive study on the compressive strength, durability-related parameters and microstructure of geopolymer mortars based on mixed construction and demolition waste

A comprehensive study on the compressive strength, durability-related parameters and microstructure of geopolymer mortars based on mixed construction and demolition waste

Emircan Ozcelikci [a,b], Anil Kul [a,b], Muhammed Faruk Gunal [a], Behlul Furkan Ozel [c], Gurkan Yildirim [a,d,*], Ashraf Ashour [d], Mustafa Sahmaran [a]

[a] *Department of Civil Engineering, Hacettepe University, Ankara, Turkey*
[b] *Institute of Science, Hacettepe University, Beytepe, Ankara, Turkey*
[c] *Department of Civil Engineering, Yozgat Bozok University, Yozgat, Turkey*
[d] *Department of Civil and Structural Engineering, University of Bradford, Bradford, UK*

ARTICLE INFO

ABSTRACT

As a viable option to upcycle construction and demolition waste (CDW) into value-added materials, geopolymer technology is emerging. Most studies investigate CDWs in a separated form or in combination with mainstream pozzolanic/cementitious materials focusing only on fundamental properties of geopolymer pastes, not considering to scale such materials to the level of their application in the forms of structural mortars/concretes or to characterize long-term performance/durability. This study investigated the development and characterization of ambient-cured mortars with mixed CDW-based geopolymer binders and untreated fine recycled concrete aggregates (FRCA). Mixture of CDW-based roof tile (RT), red clay brick (RCB), hollow brick (HB), concrete (C), and glass (G) was used as the precursor, while ground granulated blast furnace slag (S) was used in some mixtures to partly replace CDW precursors. Compressive strength, durability-related parameters including drying shrinkage, water absorption, and efflorescence, microstructure and materials sustainability were evaluated. Results showed that 28 d compressive strength results above 30 and 50 MPa are achievable with the entirely CDW-based and slag-substituted mortars, which were found improvable to have entirely CDW-based structural concretes. Drying shrinkage of the mortars is slightly higher than that of conventional cementitious/geopolymeric systems although it can be minimized significantly through mixture optimization. Water absorption values remain comparable with the literature. CDW-based geopolymer mortars outperform Portland cement mortars in terms of CO_2 emission and energy requirement. Our findings show that via utilizing CDW-based constituents in mixed form as precursor and waste aggregates, it is possible to develop greener construction materials with acceptable strength and long-term performance.

1. Introduction

The construction industry accounts for at least 42% of total energy consumption in Europe and 35% of the total greenhouse gas emissions (Nguyen et al., 2021). The production of cement, the main binder of traditional concrete, is responsible for the consumption of 3.2–6.3 GJ of energy and 1.7 t of raw materials per t of clinker alone, leading to significant rates of greenhouse gas emissions (Rahman et al., 2015). Cement production is also quite inefficient as 40% of the energy is wasted during the production process (Verma et al., 2021). Energy inefficiency and non-eco-friendliness of the construction industry are the issues that need to be addressed not only from the perspective of production and construction but also from the perspective of demolition of the aged infrastructure that has completed their service life. This is where the issue of generation of construction and demolition wastes (CDWs) resulting from the new construction practices, infrastructural development, repair/maintenance/renovation applications, and demolition works becomes important and needs to be rigorously considered. CDWs constitute 25–30% of the total waste generated in the EU (European Commission, 2019), and every year, around 800 Mt of CDW are

generated in Europe (Wu et al., 2019). Solutions focusing on the reduction of cement-based materials and enhancement of recyclability can multiply the benefits sustainability-wise. To that end, geopolymers/alkali-activated materials, which can possibly replace traditional building materials and enable the recycling of end-of-life materials such as CDWs, have come to the fore (Dadsetan et al., 2019).

Geopolymers/alkali-activated materials are greener options than traditional cement-based materials and commonly produced by activating aluminosilicate industrial wastes (source materials [*i.e.*, precursors]) with alkali metal hydroxides and silicates (Provis et al., 2005). Although common industrial wastes/by-products (*e.g.*, different classes of fly ash and ground granulated blast furnace slag) are widely used in producing geopolymers, they are highly demanded by the cement and concrete industry. Many research investigations have focused on producing geopolymers from different source materials. CDWs have great alkaline activation potential given their aluminosilicate-rich nature, although the number of studies evaluating CDWs performance in geopolymer synthesis is quite limited compared to abovementioned mainstream precursors. It has been shown that individual fractions of CDW-based materials such as tiles (Yildirim et al., 2021), bricks (Tuyan et al., 2018), glass (Ulugöl et al., 2021a), concrete (Robayo-Salazar et al., 2017), unbound aggregates (Bassani et al., 2019) can successfully be used in geopolymerization. Despite their well identified potential for use in alkali-activated systems, most of the related studies focused on the volarization of CDWs in blends with mainstream precursors/traditional cement and/or under high temperature curing, which limits the technological transfer and is not desirable for the sake of maximizing CDW upcycling ratio (Robayo-Salazar et al., 2020). The need for combined utilization of CDW-based precursors together with mainstream pozzolanic/cementitious materials is largely attributed to the low-to-medium pozzolanicity (*i.e.*, reactivity) of CDW-based materials (Frías et al., 2020), which becomes even more challenging when combined utilization of individual CDW fractions in alkali-activation is targeted given the wide diversity of the constituents. To ensure the representativeness of the raw materials and be able to make comparative assessments with the literature studies, it is highly desirable to work on samples with wide variety of CDW constituents. When samples of unseperated CDW in former studies are evaluated, it can be observed in most cases that concrete, unbound aggregates, bricks/tiles, and glass collectively form the bulk waste composition in different regions (Tan et al., 2022a). Combined use of these wastes should be focused on future studies, although there are very limited number of studies available in literature with the focus of utilizing CDW constituents in a such a combined form in alkaline activation. In such a study, Moreno-Maroto et al. (2022) tried utilizing CDW with low amorphousness and Al_2O_3 content for geopolymerization. As different parameters to study, type/proportion of alkaline activators (sodium hydroxide [NaOH] and sodium silicate [Na_2SiO_3]), curing conditions, duration, and temperature, time of initial treatment and addition of ordinary Portland cement were considered. It was concluded that the reactivity of obtained samples was low leading to relatively low strength levels and efflorescence formation. Only with temperature curing (60–90 °C) and dry/sealed curing, meaningful compressive strength results were obtainable. Portland cement utilization led to certain improvements in the compressive strength but also caused greater efflorescence, which was reported as an important research topic to research further. Tan et al. (2022a) focused on the feasibility of using unseparated CDW incorporating unbound aggregates, red clay bricks, waste concrete, waste tiles and waste glass as precursors in different combinations in geopolymer production. The effect of different combinations of separate CDW components on the reactivity of mixed CDW and performance of unseparated CDW-based geopolymer was investigated. The samples were activated with large share of sodium silicate (Na_2SiO_3) and some amount of sodium hydroxide (NaOH) and cured in an oven set at 50 °C for 7 days. Their findings showed that it is possible to have reactive phases and highly reactive bonds when unseparated CDW is used for geopolymerization. It

was possible to reach compressive strength level of 29.7 MPa after 7 days and the increased contents of unbound aggregates and waste concrete led to the achievement of geopolymers with higher strength while an opposite trend was noted when the content of red clay brick was increased. In another work of Tan et al. (2022b), the effect of milling duration (1, 2, 3, and 4 h) on the reactivity of unseparated CDW (composed mainly of wastes of concrete, unbound aggregates, red clay bricks, tiles, and glass) and resulting geopolymer mixtures were evaluated. Geopolymers were manufactured by using a mixture of Na_2SiO_3 and NaOH as the alkaline activators and cured at 50 °C in an oven for 7 and 28 days, before being tested for compressive strength. According to the results, with the increased milling duration, particle size, crystallinity, surface group of the CDW precursors change promoting improved rates of reaction and denser microstructure. It is suggested not to extend the milling duration beyond 2 h. After 2 h of milling, 28-day compressive strength in the range of 35 MPa was achieved, and only minimal changes took place with the prolonged milling durations. Tan et al. (2022c) also focused on the efflorescence behavior of unseparated CDW-based geopolymers activated by a mixture of Na_2SiO_3 and NaOH, and efflorescence mitigation was aimed by using either slag or metakaolin. It was concluded that both metakaolin and slag was very effective in mitigating efflorescence formation, although the mechanisms being involved in mitigation were different for different mineral admixtures. 28-day compressive strength of air cured geopolymers with no mineral admixtures was found to be in the range of 8 MPa but with the addition of metakaolin and slag, results markedly improved exceeding 30 MPa depending on the rate of use of these materials.

Recycling CDW in a mixed form is complicated considering the wide variations in the proportion of the constituents, which can closely affect the ultimate geopolymer material due to differences in the chemical composition, fineness, amorphousness, and other related properties of the constituents (Tan et al., 2022a). According to Alhawat et al. (2022), clayey CDWs such as bricks and tiles incorporate higher levels of SiO_2 and Al_2O_3 compared to other CDWs, which is expected to lead to geopolymeric gels with more Si–O–Al bonds (Komnitsas et al., 2015). Presence of calcium ions in an optimal range, which is largely related to the proportion of waste concrete in the CDW, was shown to positively affect the resultant geopolymer material (Alventosa and White, 2021). To achieve an ideal geopolymerization, it is critical to balance the CDW constituents (relatedly the oxide/mineral composition). Related to CDW utilization in geopolymerization, the literature is greatly lacking not only in terms of the effect of type/fraction of CDW constituents but also the selection of alkaline activators with proper type/combination, achieving reasonable compressive strength and setting clear curing conditions/durations (especially ambient) (Tan et al., 2022a). Although valuable, majority of the related studies are on the assessment of fundamental properties (i.e., strength measurements and microstructural characterization) of CDW-based geopolymer materials, while there are almost no studies available in the literature, which focus on the scaling of such materials to the level of their application in the forms of mortars, concretes, construction elements, and/or applications together with the long-term performance characterization and durability (Robayo-Salazar et al., 2020).

The main purpose of the current study is to develop and characterize completely CDW-based geopolymer mortars with reasonable compressive strength levels that can be scaled up to the strength levels (i.e., in the range of 30 MPa) of completely CDW-based concrete mixtures suitable for use in large-scale structural components for the planned future works. Different from most of the literature studies, emphasis was placed on the achievement of high compressive strength levels under ambient curing conditions for the mixtures with geopolymer pastes having mixed CDW-based precursors with no further treatment to modify their oxide/mineral composition and crystallographic nature and fine recycled concrete aggregates (FRCA). High compressive strength levels for the mortars were aimed not to jeopardize the compressive strength of CDW-based structural concrete mixtures planned to be developed in future,

presuming that there would be further decrements in the strength with the addition of coarse recycled concrete aggregates. Through using waste concrete as fine recycled aggregates, the aim was to maximize the amount of CDW utilized, reduce raw/clean materials usage, and upcycle FRCA, which has been mostly downcycled and recommended for use in low-grade non-structural applications by most of the past studies (Villagrán-Zaccardi et al., 2022). As another novel aspect, parameters (*i.e.*, drying shrinkage, efflorescence, water absorption) that are closely related and critical to the durability and long-term performance of completely CDW-based geopolymer mortars (and relatedly concretes) were focused for the first time in literature to the authors' best knowledge. Comprehensive microstructural analyses including scanning electron microscopy with energy dispersive X-ray spectroscopy (SEM/EDX), thermogravimetry (TG/DTG), mercury intrusion porosimetry (MIP), and nuclear magnetic resonance (NMR) spectroscopy were also made to validate and correlate the results along with the sustainability analyses based on the material sustainability index (MSI) approach.

2. Experimental program

2.1. Materials

2.1.1. Collection and preparation of CDW-based precursors

In this study, CDW-based materials were used as precursors to obtain geopolymer binders which were then incorporated with the CDW-based fine recycled concrete aggregates (FRCA) to obtain geopolymer mortars ultimately. In half of the mixtures, ground granulated blast furnace slag (S) was substituted with some part of the CDW-based precursors to see the effect of higher calcium content on the overall performance. Different CDWs used herein were roof tile (RT), red clay brick (RCB), hollow brick (HB), concrete (C), and glass (G), which were obtained from an old, demolished structure situated in an urban transformation area with selective demolition practices. The type and proportions (as will be discussed) of CDWs were agreed to achieve ideal geopolymerization and high compressive strength results under ambient curing conditions considering authors' previous experience (Ulugöl et al., 2021a). Each CDW-based material was subjected to a 2-step crushing and milling procedure for powderization. Each one of the
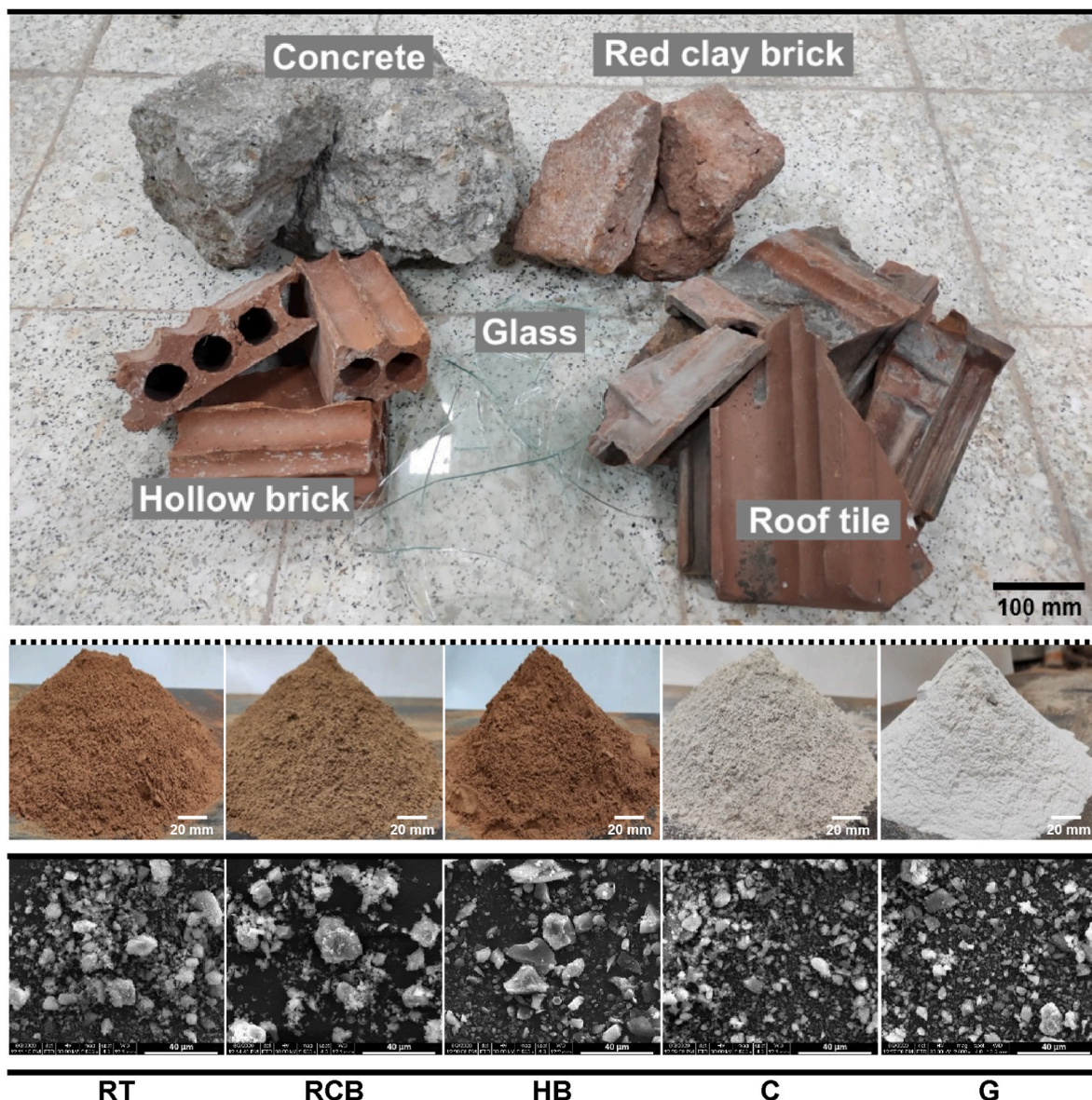

Fig. 1. Video camera and SEM images of the precursors before and after grinding. (The scales in SEM images are 40 μm).

materials was crushed by a jaw crusher with 1 mm spacing and then was ground in a ball mill for an hour. Due to their diverse nature, CDWs had different particle size distributions, surface characteristics, and crystalline nature, but no special attention was paid to have the materials with similar grain size distributions to better simulate the real-life cases of construction and demolition. Upon demolition of a structure, different types of CDWs are obtained together. It takes substantially less work to recycle different types of CDW materials together. As this situation was foreseen, all materials were crushed and milled under the same conditions (*i.e.*, same crusher spacing, milling duration, and ball configuration) in the study. The video camera and scanning electron microscope (SEM) images of different precursors were presented in Fig. 1. According to the SEM images, clayey precursors (*i.e.*, HB, RCB, and RT) were similar to each other and mostly with angular grains having rough surface, whereas C and G had a mixed particle structure that included grains with both angular and smooth surface. Impurities were much clearer in the case of C compared to other precursors due to hydrated cement/mortar residues on the grains.

2.1.2. Characterization of CDW-based precursors

The gradation curves and chemical compositions (as determined by X-ray fluorescence [XRF] analysis) of the precursors are shown in Fig. 2 and Table 1. Table 1 also presents the characteristic dimensional properties such as surface weighted mean diameter (D[3,2]), volume weighted mean diameter (D[4,3]), and particle diameters of materials indicating the size below which 10% (d(0,1)), 50% (d(0,5)), and 90% (d(0,9)) of all particles are found, by mass. According to Komnitsas et al. (2015), significant improvements in the mechanical properties of geopolymers can be obtained when fractions having d(0,5)<15 μm are used. As seen in Table 1, all precursors except G have a smaller fraction than this threshold value. After the most efficient grinding period which was determined as 1 h based on the previous experience of the authors, the smallest average particle size among different CDWs belonged to clayey precursors, whereas the average particle size of G was the coarsest.

As seen from Table 1, the chemical compositions of the clayey CDWs were quite similar with minor differences. They were rich in siliceous and aluminous oxides, which are essentially important for geopolymerization (Duxson et al., 2007). C had the greatest CaO level (21.2%) among all CDWs most probably due to the presence of old adhered mortar and calcareous aggregates in its composition. G was the richest in SiO_2 (72.5%) content among all CDWs. It was previously shown that when used singly, the geopolymerization performance of glass waste was poorer compared to different types of CDWs mostly due to low Al_2O_3 content of glass negatively affecting the Si/Al balance (Yildirim et al., 2022). It can still be considered as a valuable material considering its SiO_2-rich and amorphous nature (see below), especially when combined with other waste materials. To monitor the effect of CaO
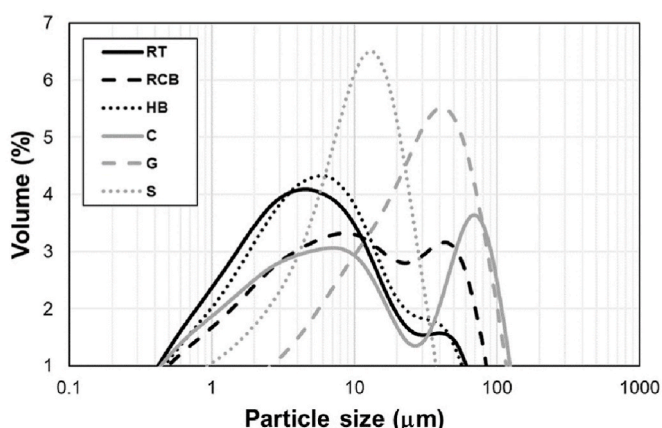
Table 1
Pyhsical properties and chemical composition of the precursors.

Physical properties	RT	RCB	HB	C	G	S
D[3,2] (μm)	2.3	2.9	2.4	2.7	6.9	3.7
D[4,3] (μm)	10.3	18.0	10.4	24.9	33.4	11.7
d(0,1) (μm)	0.8	1.1	0.9	0.9	3.5	1.6
d(0,5) (μm)	4.7	8.5	5.4	7.9	25.7	9.8
d(0,9) (μm)	28.4	51.9	28.4	79.5	75.6	24.6
Specific gravity	2.88	2.81	2.89	2.68	2.51	2.80
Chemical composition (%)						
SiO_2	49.3	52.4	53.5	37.4	72.5	32.1
Al_2O_3	20.0	19.9	19.3	10.7	0.93	11.2
Fe_2O_3	8.16	7.92	7.45	3.82	0.25	0.62
CaO	5.16	4.18	4.21	21.2	10.5	36.1
MgO	3.29	2.84	2.61	1.29	0.43	5.64
SO_3	0.79	0.95	1.46	0.54	0.24	1.21
Na_2O	1.23	1.58	1.50	1.96	12.6	0.31
K_2O	3.67	3.72	3.58	2.22	0.20	0.83
Loss on ignition	6.64	4.68	4.91	19.7	2.15	9.09

content on the performance of the final geopolymer mortars, selected mixtures were incorporated with S which was with the CaO content of 36.1%.

Crystal structures observed as a result of XRD analyses together with their particle diffraction file (PDF) numbers and chemical formula were presented in Fig. 3 and Table 2. It was observed that Quartz peaks with a broad hump centered between 2θ values of approximately 26° were detected in RT, RCB, and HB, while mainly Quartz and Calcite mixed peaks were observed in C at 26° and 29°. The detected quartz mineral is a tetrahedral structure formed between silicon atoms and oxygen that crystallizes in the hexagonal system and positively impacts the mechanical characteristics of geopolymers due to its ability to provide barriers for crack propagation (Nergis et al., 2020). Quartz, Cristobalite, Tridymite, Calcite, Albite, Diopsite, and Lazurite were the major peaks found in CDW-based precursors. The presence of these crystal structures is related to the calcination process of CDW-based materials at approximately 800–1000 °C and the formation of different crystal types during the cooling stage (Baronio and Binda, 1997). It was also seen that the crystalline structures of RT, RCB, and HB show similarity to fly ash (Palomo et al., 1999), which is one of the most frequently used source materials in the production of geopolymers in the literature. While an amorphous structure was detected for G and S, low density traces of albite crystals were found in S.

2.1.3. Preparation and characterization of fine recycled concrete aggregate

CDW-based concrete was used to obtain fine recycled concrete aggregate (FRCA) in this study. Geopolymer binders were incorporated with the fine recycled concrete aggregate without any treatment to
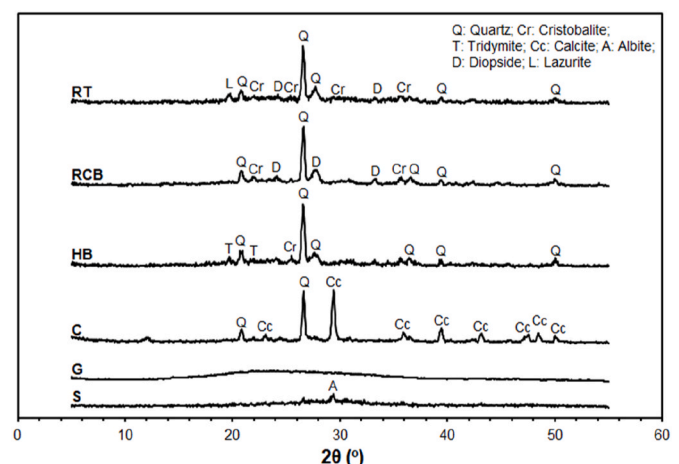

Fig. 2. Gradation curves of the precursors.

Fig. 3. X-ray diffractograms of the precursors.

Table 2

Chemical formula and PDF numbers of the crystalline phases observed in XRD analyses.

Crystalline phase	Symbol	PDF number	Chemical formula
Quartz	Q	96-901-1494	SiO_2
Cristobalite	Cr	96-900-1581	SiO_2
Tridymite	T	96-901-3394	SiO_2
Calcite	Cc	96-900-0968	$CaCO_3$
Albite	A	96-154-0705	Ca_3O_5Si
Diopside	D	96-900-1333	$Al_{0.06} Ca_{0.91} Fe_{0.1} Mg_{0.91} Na_{0.05} O_6 Si_{1.97}$
Lazurite	L	96-901-1357	$Al_{2.91} Ca_{0.6} Na_{3.48} O_{11.52} Si_{3.09}$

manufacture geopolymer mortars. Concrete waste constitutes the largest share in CDW with a ratio of about 40% (Oikonomou, 2005). It is critical to recycle waste concrete efficiently among all other CDWs. Along with using concrete waste as part of the precursors, it was used as FRCA in the mixtures to maximize its utilization rate. To obtain FRCA, concrete waste was first crushed by using a jaw crusher with 1 mm opening and then sieved through a 2 mm sieve and blended. A significant amount of crushed fine materials (0–2 mm) is acquired as a result of the recycling of CDWs. It was reported that approximately 20–40% of the fine particles are composed of 0–2 mm particles (Solyman, 2005). By using fine fractions as FRCA, it was aimed to reduce the extra processing of CDW-based materials and pollutive dust formation. A large share of fine particles of FRCA is expected to cause an increase in the water requirement of the mixtures to ensure sufficient workability, although it was considered that when adequate workability is provided, the presence of FRCA will provide a certain reactivity and filling effect in the geopolymer mortars. The particle size distribution of the FRCA was shown in Fig. 4. The proportion of aggregates below 106 μm constitutes approximately 22.8% of the total weight of the aggregates (Fig. 4), which can be considered beneficial to obtain a denser matrix and improved mechanical performance. FRCA was with the compacted unit weight of 1352.5 kg/m³, loose unit weight of 1273.3 kg/m³, dry specific gravity of 1.95, saturated surface dry specific gravity of 2.17, apparent specific gravity of 2.50, water absorption of 11.1% and porosity of 21.7%.

2.2. Mixture design

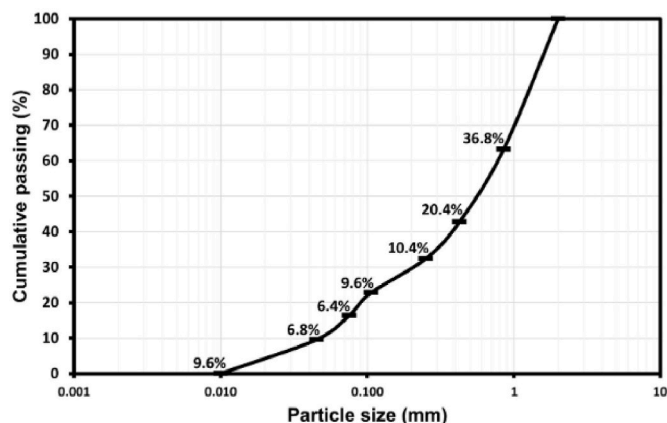As a result of the preliminary trials, six mortar mixtures were

Fig. 4. Particle size distribution and range of FCRA.

designed to evaluate the key parameters affecting the performance of the final products. The proportions of CDW-based geopolymer mortar mixtures were shown in Table 3. For the valorization of CDW-based components together, mixed CDW with the combination of 30% RT, 17% RCB, 23% HB, 10% G and 20% C was used as precursors in producing the mixtures, which were decided based on a previous experience (Ulugöl et al., 2021b). The mixtures coded as "CGM-1, CGM-2, and CGM-3" consisted of completely CDW-based materials, while the mixtures coded as "CGM-1/S, CGM-2/S, and CGM-3/S" were identical to previous mixtures although the total amount of CDW-based precursors were replaced with the use of S, by 20%. Water/binder and FRCA/-binder ratios were kept constant at 0.35 in all mixtures. FRCA was expected to reduce the compressive strength results of mixed CDW-based geopolymers given its nature, which led authors to keep its utilization rate constant. It is important to have reasonable strength results in the presence of FRCA, utilization of which is mostly limited to low-grade non-structural applications (Villagrán-Zaccardi et al., 2022). Although the amount of FRCA was constant, through their utilization, it was also aimed to reveal the successful usability of FRCA in completely mixed CDW-based geopolymers without risking the compressive strength results and increase their upcycling potential. It is important to note that the utilization of CDW-based aggregates in CDW-based geopolymers with different properties require further research efforts, although this is not focused herein.

To dissolve aluminosilicate-based precursors in an alkaline environment, sodium hydroxide (NaOH) was used in all mixtures (Xu and Van Deventer, 2000). Geopolymerization reactions are known to accelerate by the combined use of alkali hydroxides and soluble silicates (Palomo et al., 1999). For this reason, sodium silicate (Na_2SiO_3), in the liquid form, was used as another alkaline activator. Amount of water used in the mixtures was calculated considering the water content of Na_2SiO_3. Together with NaOH and Na_2SiO_3, certain mixtures contained calcium hydroxide ($Ca(OH)_2$) as an additional activator. One of the main reasons of adding calcium-based components to the geopolymer systems was to achieve increased compressive strength levels under ambient conditions (Temuujin et al., 2009). The alkaline activator type and concentration is one of the most important aspects together with the type/properties of the aluminosilicate precursors in geopolymer systems. Several alkaline activator combinations were planned and used during the design of the mixture proportions of mortar mixtures. Regardless of the type of precursors, the combination of the alkaline activators used in the mixtures was divided into three groups. In the first group (CGM-1/S and CGM-1), NaOH with the Na concentration of 6%, by the total weight of the binder was used alongside with the Na_2SiO_3 having twice the weight of the NaOH used. In the second group (CGM-2/S and CGM-2), along with the alkali activator combination of the first group, $Ca(OH)_2$ by 2% of the total weight of the binder was used. In the third group (CGM-3/S and CGM-3), NaOH with the Na concentration of 10%, by the total weight of the binder was used

Table 3

Mixture designs of CDW-based geopolymer mortars.

Ratios of ingredients	Mixture ID					
	CGM-1/S	CGM-1	CGM-2/S	CGM-2	CGM-3/S	CGM-3
Precursors (%)						
Mixed CDW	80	100	80	100	80	100
Slag (S)	20	–	20	–	20	–
Aggregate, by the total weight of the precursor (%)						
FRCA	35	35	35	35	35	35
Alkaline solutions, by the total weight of the precursor (%)						
Water	35	35	35	35	35	35
Na	6	6	6	6	10	10
NaOH	10.44	10.44	10.44	10.44	17.40	17.40
Na_2SiO_3	20.88	20.88	20.88	20.88	–	–
$Ca(OH)_2$	–	–	2	2	6	6

together with the Ca(OH)$_2$, by 6% of the total weight of the binder.

All mixtures were prepared by using the same mixing procedure, which included the following steps: (i) NaOH solution was prepared 24 h prior to mixing and kept to cool down to the room temperature, considering the workability losses that might be caused by the exothermic reactions between NaOH and water (Rashidian-Dezfouli and Rangaraju, 2017), (ii) dry mix consisting of CDW-based precursors and FCRA was mixed for 60 s at 100 rpm by a mortar mixer, (iii) Subsequently, the NaOH solution was slowly added to the mixer in 60 s and mixed for an additional 120 s at 100 rpm, (iv) during mixing, Na$_2$SiO$_3$ solution, if found in the mixture design, was added to the mixture in 60 s and the mixing process was continued for 120 s at 150 rpm, (v) Ca(OH)$_2$, if found in the mixture design, was added to the system in 60 s after the addition of Na$_2$SiO$_3$ and mixed for another 180 s at 150 rpm.

2.3. Curing and testing

In the current study, three cubic specimens with $50 \times 50 \times 50$ mm dimensions were prepared for each of the CDW-based geopolymer mortar mixtures to specify the compressive strength results at the ages of 7 d, 28 d, and 90 d. After initial casting, the samples were kept in their mold with their surfaces covered for 24 h under ambient conditions set at average temperature of $23 \pm 2\ °C$ and a relative humidity of $50 \pm 5\%$, and then moved into plastic bags having controlled environment set at average temperature of $23 \pm 2\ °C$ and relative humidity of $95 \pm 5\%$ until the testing date. Compressive strength tests were performed at a loading rate of 0.9 kN/s by using a 100-t capacity testing device in accordance with the ASTM C109 (2020) standard. The compressive strength result was calculated by averaging the results obtained from three separate specimens tested.

Drying shrinkage tests were performed in accordance with the ASTM C596 (2018) standard. For this test, three prismatic specimens measuring $25 \times 25 \times 285$ mm (height × width × length) were prepared to be tested at predetermined ages for each of the mortar mixtures. The length measurements were performed until the end of 7 d, 14 d, 28 d, and 90 d. Before the tests, specimens were first kept in water at temperature of $23 \pm 2\ °C$ for two days. Afterwards, they were left in an ambient environment with the average temperature of $23 \pm 2\ °C$ and relative humidity of $50 \pm 5\%$ until the test day. The length measurements were then performed for the specimens removed from the water and a comparator was used to determine the level of shrinkage of the specimens. Changes in the length measurements were calculated using Eq. (1).

$$Microstrain = \frac{L_x - L_i}{L_i} \times 10^6 \qquad (1)$$

where, L_i represents the initial measurement length (length of specimen + two pins attached to both ends of the specimens), L_x represents the length of the specimen at the age of testing.

Water absorption test under atmospheric pressure was performed on the mortar mixtures in accordance with the ASTM C642 (2013) standard. Water absorption test measures the change in the mass of the saturated specimen by allowing it to absorb water. In this test, three cylindrical specimens measuring 50 mm in thickness and 100 mm in diameter (Ø100 × 50 mm) were prepared for each mixture to determine the water absorption values. The specimens were first left to dry in an oven at $50 \pm 5\ °C$ for two days until they reached to a constant weight. Afterwards, they were kept under laboratory conditions ($50 \pm 5\%$ relative humidity, $23 \pm 2\ °C$ temperature) for 6 h and their weights were recorded. After drying, all cylindrical specimens were submergerd in water. The specimens were removed from the water after 24 h and weight recordings after their surfaces dried were made and water absorption results were determined. The water absorption was calculated using Eq. (2).

$$Water\ absorption\ (\%) = \frac{w_{ssd} - w_d}{w_d} \times 100 \qquad (2)$$

where, w_{ssd} represents the saturated surface dry weight of the specimen, and w_d represents the dry weight of the specimen.

Efflorescence formation was evaluated by using a single 50 mm-cubic specimen which was kept under laboratory conditions ($50 \pm 5\%$ relative humidity, $23 \pm 2\ °C$ temperature) for 90 d. The specimens were visually examined considering the intensity of the white-colored products formed on the surface of the specimens because of the efflorescence formation. SEM/EDX and X-ray diffraction analyses (XRD) were performed to characterize the efflorescence products.

Along with the abovementioned tests, in-depth microstructural analyzes were performed on 90 d old mortar specimens. For the characterization of microstructure, reaction products and elemental distribution, SEM/EDX analysis was performed. Mortar samples with the dimensions less than 1 cm were used for this analysis. XRD analyses were performed at a scan range of $5° \leq 2\theta \leq 55°$, with a 2θ step length of 0.033°, scanning step time of 30.48 s and for the wavelength Kα1 of copper ($\lambda = 1.5406$ Å) to illustrate the composition of the efflorescence products. Powder samples weighing nearly 15 mg were scratched and used for the XRD analyses. Thermogravimetric (TG/DTG) analyses were performed using 15 mg powder samples at temperatures ranging from 25 to 1000 °C with an incremental rate of 10 °C/min to determine the degradation temperatures of the samples. The degradation temperatures and degrees of the chemically/physically bound water and/or geopolymeric bond structure of the samples were assessed by using the thermograms generated from these analyses. Mercury intrusion porosimetry (MIP) analyses were performed to measure the void distribution and pore structure of the mortars. During the MIP analyses, γ was the surface tension of the mercury and θ was the contact angle between the mercury and the pore wall, which were 480 erg/cm^2 and 140°. A device capable of applying pressures up to 50,000 psi (approximately 345 MPa) was used in MIP analysis. At last, nuclear magnetic resonance (NMR) spectroscopy was performed on the mortar samples to reveal the chemical and structural characteristics on the molecular basis, which include the identification of the main geopolymerization products and atomic bond structure. Since the main reaction products of geopolymers are Al and Si-based gel structures, ^{29}Si and ^{27}Al NMR analyses were performed on the samples.

Apart from the detailed tests and analyses listed above, the greenness of the developed mixtures was discussed quantitively in comparison to ordinary Portland cement-based systems, following the material sustainability index (MSI) approach.

3. Results and discussion

3.1. Compressive strength

Average compressive strength results of CDW-based geopolymer mortars at the end of 7 d, 28 d and 90 d ambient curing were presented in Fig. 5. After 7 d of ambient curing, the results were 18.2, 20.9, and 10.3 MPa for entirely CDW-based CGM-1, CGM-2, and CGM-3 mixtures, and 26.0, 34.4, and 13.1 MPa for slag-substituted CGM-1/S, CGM-2/S, and CGM-3/S mixtures. Similar trend was noted for later-age results. After 90 d of ambient curing, the results of entirely CDW-based CGM-1, CGM-2, and CGM-3 mixtures were 31.3, 35.1, and 28.2 MPa, and 43.8, 56.4, and 33.7 MPa, for slag-substituted CGM-1/S, CGM-2/S, and CGM-3/S mixtures. Irrespective of the different mixture proportions and curing ages, the individual compressive strength results obtained from separate cubic specimens were close to each other so that standard deviations did not exceed 3.08 MPa. The compressive strength results were observed to be highly dependent on the slag substitution and combination of the alkaline activators. For example, slag substitution by 20% led 39.9% improvement in the 90 d average compressive strength of
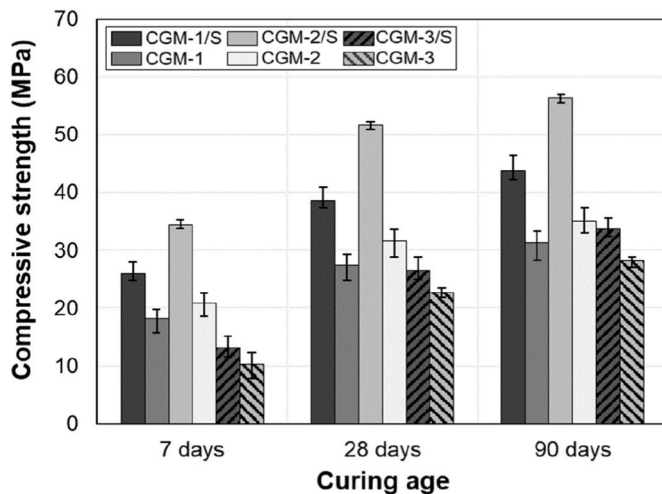
Fig. 5. Average compressive strength results of CDW-based geopolymer mortars after different curing ages.

geopolymer mortars with the combined use of NaOH + Na_2SiO_3 (CGM-1/S, CGM-1), while the improvement rates were 60.6% and 19.5% for mixtures with the combined use of NaOH+Na_2SiO_3+$Ca(OH)_2$ (CGM-2/S, CGM-2), and NaOH+$Ca(OH)_2$ (CGM-3/S, CGM-3). The improvements noted in the compressive strength results with the inclusion of slag into the designs of entirely CDW-based geopolymer mortars were mostly attributed to the increased reactivity and high calcium content of slag (Nath and Sarker, 2014). It was reported in literature that the dominant reaction products observed in the CDW-based geopolymers is sodium alumino-silicate hydrate (NASH) gels (Mahmoodi et al., 2020). It was also reported that the main reaction products of geopolymer systems incorporating slag were calcium silicate hydrate (CSH) and calcium alumino-silicate hydrate (CASH) gel structures (Escalante-García et al., 2003). Depending on the composition of precursors and alkaline activator combinations, both NASH and CASH gels can be present in the same alkali-activated matrix as well (Garcia-Lodeiro et al., 2011). Marked improvements in the compressive strength results in the presence of slag are most likely related to the formation of calcium-based (*i. e.*, CSH and CASH) gel structures alongside with the NASH gels leading to a denser and more compact microstructure. In the presence of calcium ions in a highly alkaline medium, the NASH gel structure has an ion exchange tendency leading to the formation of an intertwined gel too (*i. e.*, [C(N)ASH]) (Garcia-Lodeiro et al., 2011). Considering the above-mentioned advantages and experimental findings, it is also important to note that the presence of slag accelerates geopolymerization reactions and enables the CDW-based matrix to form strength-giving gel structures at ambient temperature. In general, our findings indicate that the compressive strength performance of the mortars is enhanced with the addition of slag. Nevertheless, it is worth noting that after 28 d of ambient curing, even the mortars with completely CDW-based ingredients achieved compressive strengths in the range of 22.6–31.6 MPa. This compressive strength range is suitable for a wide variety of common construction applications, although our findings need to be furthered to achieve similar or better compressive strength levels in the presence of coarse aggregates for concrete mixtures rather than mortars, which will be focused in the future.

Another parameter which was decisive on the compressive strength results was different alkaline activator combinations. For example, differences in the alkaline activator combinations caused 12.1–24.5% change in the 90 d compressive strength results of completely CDW-based geopolymer mortars and 28.8–67.4% change in the same-age companion mixtures with slag substitution. For all ages, the highest compressive strength results were obtained from CGM-2/S coded mixture for the slag-substituted mixtures and from CGM-2 coded

mixture for entirely CDW-based mixtures, in which NaOH + Na_2SiO_3+$Ca(OH)_2$ combination was used together as the alkaline activator. The performance of these mixtures was followed by CGM-1/S and CGM-1 mixtures. This showed that mixtures incorporating Na_2SiO_3 in the alkaline activator combination outperformed in terms of compressive strength. Higher strength results achieved in the presence of Na_2SiO_3 was attributed to the increased availability of soluble silicates in the systems which enhance the geopolymerization kinetics by increasing reactivity of the CDW-based particles (Palomo et al., 1999). Weaker compressive strength performance observed for the mixtures with NaOH + $Ca(OH)_2$ combination might be associated with the deceleration of the ion transfer in the matrices and retardation of polymerization due to high NaOH content (Alonso and Palomo, 2001) and inadequate capacity of NaOH in dissolving CDW-based precursors.

3.2. Drying shrinkage

Drying shrinkage results of the mortars at the end of different curing ages under ambient conditions were presented in Fig. 6. The standard deviations of the obtained drying shrinkage results were close to each other regardless of the curing age and mixture type, not exceeding 988.7 με. In general, with the use of Na_2SiO_3 in the mixture compositions, higher rates of shrinkage were noted. To exemplify, while the mixtures with Na_2SiO_3 (CGM-1/S, CGM-1, CGM-2/S, CGM-2) showed drying shrinkage in the range of 12,530-19510 με after 90 d, the same range for the mixtures without Na_2SiO_3 (CGM-3/S, CGM-3) was approximately 5330–5730 με. A similar trend was also valid for other testing ages. Increased shrinkage rates caused in the presence of Na_2SiO_3 imply for a relationship between the shrinkage characteristics and rapid hardening with high brittleness (Atiş et al., 2009). Drying shrinkage mechanism of alkali-activated materials/geopolymers was reported to be mainly dependent on the use of calcium-based precursors (Thomas et al., 2012) and curing conditions (Marjanović et al., 2015), although the use of Na_2SiO_3 and related variations in the silicate modules seem to have more eye-catching effect on the general drying shrinkage behavior of the mortars in this study (Fig. 6) (Taghvayi et al., 2018). During geopolymerization, the formation of silica-rich gels, which contain high amounts of water, takes place in Na_2SiO_3-activated systems. Higher drying shrinkage of the Na_2SiO_3-activated systems can be explained by the higher rates of water loss over time from the abovementioned silica-rich gels (Matalkah et al., 2019). It was reported that the release of free water trapped in the silica gels over time also causes the onset of shrinkage (Zhang et al., 2022). In line with these results, it has also been reported that the activation with Na_2SiO_3 causes smaller porosity and fine pore sizes than activation with NaOH and an increase in drying shrinkage due to growing tensile stress localization in the capillary pores (Taghvayi et al., 2018).
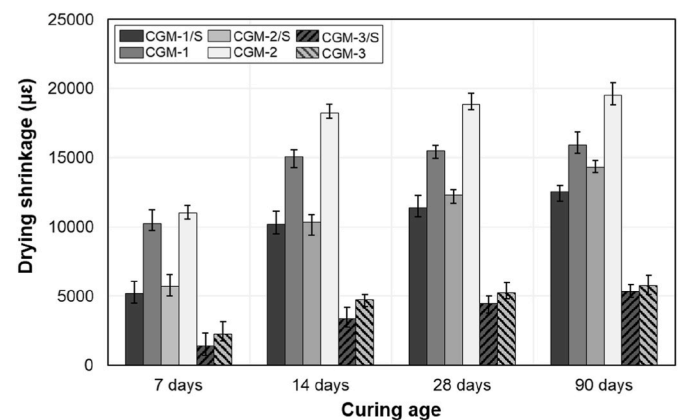

Fig. 6. Drying shrinkage results of CDW-based geopolymer mortars after different curing ages.

It was clearly seen from the results that, regardless of the mixture design, early-age shrinkage was critical so that most of the drying shrinkage strains occurred during the first 14 d and the subsequent time-dependent increments were lower especially beyond 28 d. This high shrinkage rate during the first 14 d was associated with the excessive water release and evaporation during geopolymerization reactions, as also reported in the study of Wallah and Rangan (2006). In the work of Collins and Sanjayan (2000), Portland cement-based concrete as the control specimen showed lower drying shrinkage than that of alkali-activated slag concrete despite having higher weight loss during drying. It was concluded that water loss was not the only parameter affecting the drying shrinkage behavior of the alkali-activated materials/geopolymers but the pore size distribution and geopolymer gel characteristics were also highly effective as will be detailed in the following sections. They concluded that the drying shrinkage behavior of the alkali-activated materials is also driven by the capillary tensile forces formed during rapid hardening of mixtures with Na_2SiO_3 at the drying state. Considering the shrinkage behavior of the mixtures containing Na_2SiO_3 (CGM-1/S, CGM-1, CGM-2/S, CGM-2), it was observed that the slag-containing mixtures showed a lower shrinkage than the slag-free mixtures. Similar behavior was also noted for CGM-1/S and CGM-1 mixtures without Na_2SiO_3, although the differences in the drying shrinkage results were not that different. Lower drying shrinkage strains noted for the slag-containing mixtures was mainly attributed to two reasons: (i) reduced total amount of evaporated water due to self-cementing and hydration capability of slag with the free water in mixture and (ii) reduction of interconnected capillary networks in the presence of slag (Deb et al., 2015). On top of the effects of Na_2SiO_3 and slag substitution, drying shrinkage results were also affected by the presence of $Ca(OH)_2$. For example, when the shrinkage behaviors of mixture groups of CGM-1 and CGM-2 were considered (regardless of the slag substitution), the use of $Ca(OH)_2$ as a tertiary activator increased the level of drying shrinkage. Although there are findings in literature which state that the use of $Ca(OH)_2$ causes an improvement in the shrinkage resistance of alkali-activated slags (Zhu et al., 2018), this was not the case for geopolymers with slag-substituted CDW-based precursors. It seems that the use of different alkaline activator combinations greatly affected the drying shrinkage behavior by modifying the chemistry and reaction products of mixed CDW-based geopolymer mortars.

It has been noted that unlike ordinary Portland cement, the water in the geopolymer binders is not directly incorporated into the gel structures, with a small percentage remaining as an intermediate water in the gels as will be discussed in the following sections (Tchakouté et al., 2016). In an alkali-activated binder, free water that does not participate in the gel structure can escape from the paste exposed to relatively low relative humidity conditions under ambient temperatures. As such, excessive moisture loss can cause shrinkage cracking in geopolymers. As presented in Fig. 7, drying shrinkage resulted in shallow map-type microcracks on the specimen surface. For different mixtures, formation of microcracks due to drying shrinkage varied randomly and was independent from the compressive strength; no direct relationship between the microcracks generated by drying shrinkage and compressive
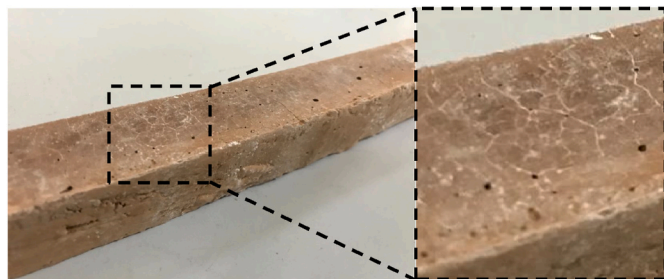

Fig. 7. Representative image of 90 d old drying shrinkage test specimen (CGM-3/S mixture).

strength results could be established, as previously reported in literature (Adesanya et al., 2018). Yet, the possible effects of microcracks formed due to drying shrinkage on the durability-related properties of the samples were further discussed in the following sections.

3.3. Water absorption

In Fig. 8, the water absorption of CDW-based geopolymer mortars at the end of 7 d, 28 d, and 90 d ambient curing were shown. Similar to compressive strength and drying shrinkage results, individual water absorption results obtained from separate specimens were close. Based on initial curing age and mixture type, the maximum standard deviation recorded was 0.57%. The water absorption was found closely dependent on the slag substitution and differences in the combined use of alkaline activators. The water absorption of slag-substituted CGM-1/S, CGM-2/S, and CGM-3/S- mixtures were lower with less standard deviation compared to slag-free CGM-1, CGM-2, and CGM-3 mixtures. For the given alkaline activator combination, slag substitution reduced the water absorption of the mixtures in the range of 30.9–34.6%. This was particularly evident with the extended ages. As also discussed under the title of compressive strength, slag substitution resulted in the acquirement of denser and more compact matrix thereby restricting the ingress of water via reduction in porosity. Similar results were also reported in literature and concluded that formation of extra CASH gels in the medium with the help of slag substitution reduces the water absorption by improving the microstructure (Bellum et al., 2020).

Among the slag-substituted mixtures (CGM-1/S, CGM-2/S, CGM-3/S), the lowest water absorption was acquired from the mixture, which was activated by the binary use of $NaOH + Ca(OH)_2$, while the mixtures activated by the binary use of $NaOH + Na_2SiO_3$ gave higher water absorption, which implies for a trend non-concordant with the compressive strength results. The same trend was also observed for entirely CDW-based mixtures (CGM-1, CGM-2, CGM-3). Accordingly, there seems to be no direct relationship between the water absorption and compressive strength development results and the water absorption is mainly affected by the volume of internal porosity including capillary and structural pores more than the compressive strength (Mobasheri et al., 2022). This statement could be more understandable by considering the MIP analyses presented in the following section.

Water absorption of all mixtures increased with the increasing age regardless of the differences in the mixture compositions (Fig. 8). This may possibly be related to the increments in the pore volume of the geopolymer structures over time. In a study by Zhang et al. (2014), pore
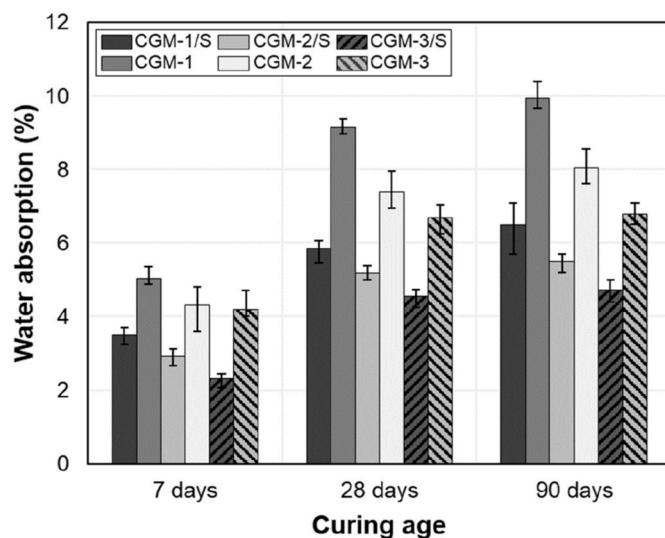

Fig. 8. Water absorption of CDW-based geopolymer mortars after different curing ages.

volume of geopolymers was reported to be capable of increasing from 6.2 to 20.6% over time. One reason for this increase may be the formation of efflorescence as the degree of efflorescence is linked to the pore structure of geopolymers. Zhou et al. (2020) reported that efflorescence increased the water absorption of geopolymers due to deterioration of pore structures by the crystallization pressure and the samples which showed efflorescence had higher pore volume and mean pore diameter than the control samples. Although the efflorescence becomes more intense when the samples are subjected to cyclic wetting and drying as in the water absorption tests, the specimens were not subjected to an intense wetting and drying conditions in this study to cause a significant amount of water absorption caused by the efflorescence (Zhang et al., 2014). Apart from efflorescence, pore structure is likely to be affected by the formation of drying shrinkage and related microcracks. It can be seen from Fig. 8 that there is a sharp increase in the water absorption results from 7 to 28 d of age, a trend of which was found quite similar to the changes monitored in the drying shrinkage strains between the same ages. Likewise, alterations in the pore structure due to drying shrinkage cracks is another reason increasing the water absorption results and it seems that water absorption results are more affected by the formation of microcracks due to drying shrinkage rather than efflorescence. The total drying shrinkage strains of the mortars were slightly higher compared to the literature studies, although the water absorption results were still found at comparable levels (Pawluczuk et al., 2021; Kaze et al., 2021; Sharma et al., 2022). It needs to be emphasized that the mortars manufactured were with a constant FRCA/binder ratio of 0.35. Although not focused herein, by making simple changes in the particle size distribution of FCRA and FRCA/binder ratio, it seems very likely to lower the drying shrinkage strains further and relatedly obtain much better water absorption results.

3.4. Efflorescence

In alkali-activated materials/geopolymers, excessive alkali ions in the system leak through the pores and interact with the CO_2 in the atmosphere; this mostly results in the formation of white salt deposits on the surface of samples. While this phenomenon, which is called efflorescence, does not affect the mechanical performance of the material in general (when it is not excessive), it implies that there are deficiencies in the matrix properties and porosity. Alkali solutions in geopolymer matrices is either chemically bound in the 3D-aluminosilicate gel or in free entrapped state in the pore solution and tend to leach from the pores to the surface, especially in low calcium/high alkali systems (Davidovits, 2008).

Different levels of efflorescence formation were observed in the mixtures containing Na_2SiO_3 (CGM-1/S, CGM-1, CGM-2/S, CGM-2) while mixtures without Na_2SiO_3 (CGM-3/S, CGM-3) almost did not show any efflorescence formation (Fig. 9). In the pore solution analysis performed by Lloyd et al. (2010), it was reported that the soluble silicates in the system will promote the reaction degree thereby limiting the alkali leaching and efflorescence. As observed, efflorescence was not only dependent on the changes in the pore solution chemistry (due to soluble silicates) but also largely on the availability of alkali metal cations in the system. As a result of the interactions of the SiO_2 of
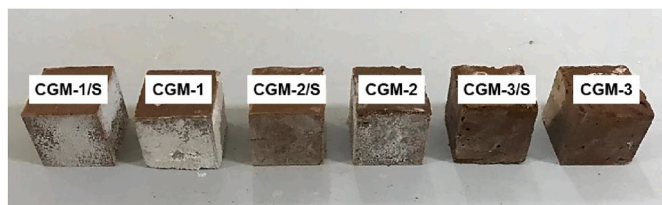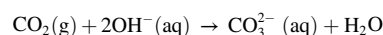

Fig. 9. Image showing the formation of efflorescence products on the CDW-based geopolymer mortars after 90 d of ambient curing.

Na_2SiO_3 with the unreacted free alkalis such as Na^+ ions, formation of weaker $Na(H_2O)_n^+$ (n indicates water molecules in the aluminosilicate matrix) bonds that can easily be broken in a humid environment takes place and efflorescence may also become pronounced (Maghsoodloorad and Allahverdi, 2016). This seems to be the case for the higher levels of efflorescence formation observed for CGM-1/S, CGM-1, and CGM-2 mixtures containing Na_2SiO_3. In CGM-2/S mixture, which contains Na_2SiO_3 and shows the best performance in terms of compressive strength, the negligible efflorescence formation is associated with the prevention of alkali leakage due to dense and compact microstructure, despite the relatively high alkalinity compared to other mixtures, except CGM-2. In highly alkaline systems, this is mainly associated with the slag substitution, which improves the matrix gel formation and restricts the pore sizes concurrently (Zhang et al., 2014). Among the mixtures containing Na_2SiO_3, due to the effect of $Ca(OH)_2$ reducing the leakage and concentration of Na^+ and leading to a more compact and denser matrix, it might have been possible to observe reduced efflorescence formation for the CGM-2/S and CGM-2 mixtures compared to CGM-1/S and CGM-1 mixtures (Tang et al., 2021).

The XRD diffractogram presented in Fig. 10 illustrates the composition of the efflorescence products. Na^+ and OH^- ions available in the matrices are considered to be the two principal factors leading to efflorescence by leaching via formation of hydrous alkali carbonates, $Na_2CO_3 \cdot 7H_2O$ (*i.e.*, natrite [N], PDF: 96-901-1305), in white crystal form due to a series of reactions with the atmospheric CO_2, details of which were given in the following equations:

$$CO_2(g) + 2OH^-(aq) \rightarrow CO_3^{2-}(aq) + H_2O$$

$$2Na^+(aq) + CO_3^{2-}(aq) + 7H_2O \rightarrow Na_2CO_3 \cdot 7H_2O(s)$$

(Zhang et al., 2014) SEM image coupled with the EDX analysis also details the efflorescence products (Fig. 10). As seen from Fig. 10-b, formation of natrite was validated in the form of elongated crystals, together with the elemental analysis complying with the XRD findings (Ulugöl et al., 2021b). Nevertheless, considering the CGM-2/S mixture which exhibited the highest compressive strength with no remarkable efflorescence formation, it seems very likely to eliminate the efflorescence problem almost completely via further tailoring of the mixture designs.

3.5. Microstructural characterization

3.5.1. Scanning electron microscopy/energy-dispersive X-ray spectroscopy (SEM/EDX)

SEM/EDX analyses were performed on the selected specimens of CGM-2/S mixture after 90 d of ambient curing, which resulted in the highest compressive strength results and likely to have formations of both Na- and Ca-based gel structures simultaneously in its matrix. Considering the fact that the use of calcium sources such as slag and $Ca(OH)_2$ in the compositions of geopolymer mortars significantly modified the properties (*e.g.*, strength, pore structure etc.), emphasis was placed on the general evaluation of the microstructure by focusing on the differences in ultimate gel structures available in a given sample. For geopolymer mortars with the entirely CDW-based ingredients having lower amounts of calcium, the main geopolymerization products are expected to be NASH gels, while in the presence of an additional calcium source in the systems, along with the Na-based gel structures, Ca-based gel structures such as CSH, CASH and/or C(N)ASH are also expected (Garcia-Lodeiro et al., 2011). To this end, determination of microstructural differences was aimed by specifically focusing on the regions, which contain low, medium, and high contents of calcium.

In Fig. 11-a, -b, and -c, representative SEM images of CGM-2/S sample coupled with EDX analyses obtained from different regions with the low, medium and high Ca contents were presented. According to the Fig. 11-a, formation of NASH gels (Myers et al., 2015), which is
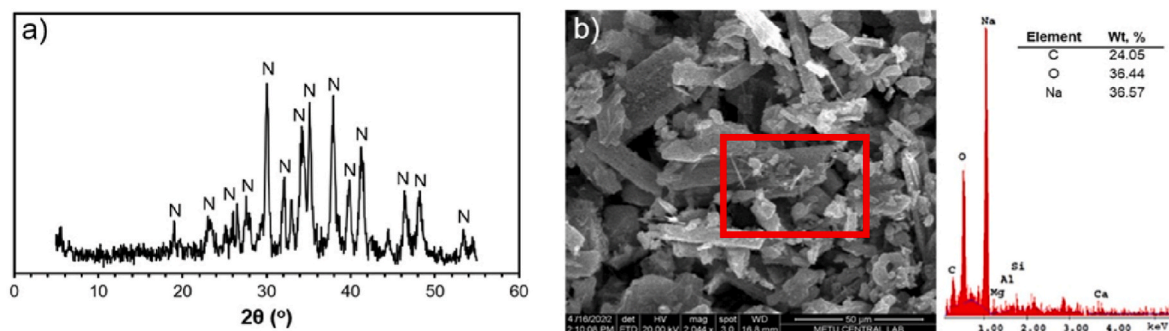
Fig. 10. (a) X-ray diffractogram and (b) SEM image with the regional EDX analysis of the efflorescence products.

the main structure responsible for strength achievement in low-Ca systems, was seen in the form of rectangular-faced and prismatic structures (Bădănoiu et al., 2015). Formation of NASH gels were also verified by the dominant elemental contents of sodium, silica, and alumina in the EDX spectra of the related region. The traces of calcium observed here can be associated with the Ca-substituted NASH gel structures with a low degree of ion exchange. In Fig. 11-b, different types of gel formation were observed most probably due to increased calcium content. Compared to low-Ca region (Fig. 11-a), the NASH structures in rectangular form mostly disappeared and replaced by more densely dispersed C(N)ASH structures. Due to hybrid gel formation with different structural order and random dispersion, the defects such as voids and microcracks were also observed similar to low-Ca regions (Fig. 11-b). As noted previously, geopolymerization reactions occur rapidly in the presence of Na_2SiO_3 and additional nucleation sites provided by the Ca^{+2} ions, which improve the polymerization and lead to denser matrices. Calcium dominated dense matrix structure obtained with the modification of the binding phase (*i.e.*, precursors and alkaline activators) can be seen from Fig. 11-c. Higher amounts of Ca in the elemental count were also indicative of Ca-based gel structures (*e.g.*, CSH, CASH and/or C(N)ASH), which was reported for the geopolymer systems supported with additional content of calcium (Temuujin et al., 2009). Similar mechanisms for the formation of abovementioned final gel structures, where the amount of Ca is a determining factor, were also reported for unseparated CDW-based geopolymers (Tan et al., 2022c).

3.5.2. Thermogravimetry (TG/DTG)

Theremogravimetry (TG) and differential thermogravimetry (DTG) plots (*i.e.*, thermograms) of geopolymer mortars in the temperature range of 30–1000 °C were presented in Fig. 12. In accordance with the majority of studies using thermal analysis in the evaluation of geopolymers, the thermograms are generally divided into three stages. Stage-I, which is in the temperature range of 0–300 °C, is associated with the dehydration of physically and chemically bound water, although latter partially occurs (Balachandra et al., 2021). According to the previous studies, the dehydration of physically bound water occurs up to the temperature range of 100–120 °C, while the dehydration of chemically bound water occurs beyond this temperature range (Ismail et al., 2014). Apart from the dehydration of water, degradations of gel structures in Stage-I were also reported (Sivasakthi and Jeyalakshmi, 2021).

In Stage-I, for all geopolymer mortars, first endothermic peaks were observed in the temperature range of 52–92 °C. The intensities of the peaks were similar for the slag-substituted mixtures; but, for completely CDW-based mixtures, the same trend did not hold true. While the weight losses were generally at similar levels, there were differences for the completely CDW-based mortars (especially for CGM-3 mixture). The weight loss corresponding to the first peak was also recorded at a higher level for the slag-substituted mixtures, which was in parallel with the literature (Hager et al., 2021). The second endothermic peak in Stage-I was detected in the temperature range of 142–161 °C with similar intensities, except for CGM-3/S which had no peak in the related range.

The total weight loss for CGM-3 was considerably higher than the other mixtures with a rate of 9.35% at the second peak. The endothermic peaks formed at this temperature range can be associated with the involvement of water into the aluminosilicate network, in other words, the conversion of water from being available at the physical state to the chemically bound state (Pu et al., 2021). Considering the differences in the abovementioned temperature ranges noted in former studies, a direct relationship could not be established between the mechanical performances and dehydration of physically/chemically bound water. This is also due to that there are two explanations for the increased availability of loosely bound water: (i) the greater amount of gel pores (micro and nano) caused by the lower density of the gel that was developed; (ii) the higher degree of gel production via more cross-linked and organized structures, which leads to higher amounts of water to be released back to the system (Ulugöl et al., 2021a). The poorer mechanical performance of CGM-3 mixture was also reflected in the thermal analysis via considerable loss in weight, which was associated with the presence of higher amounts of loosely bound water in the network due to lower rates of geopolymerization in CGM-3 mixture (Ismail et al., 2014).

In the temperature range of 300–600 °C (Stage-II), the weight loss is assigned to the dehydration and dehydroxylation of the aluminosilicate gel structure (Pu et al., 2021). As seen in Fig. 12, broad endothermic peaks were detected in the range of 430–434 °C for CDW-based geopolymer mortars, while for CGM-3/S and CGM-3 mixtures, this range was at 405–410 °C. For completely CDW-based CGM-1 and CGM-2 mixtures, weight losses were 9.81% and 9.15%, while for the slag-substituted CGM-1/S and CGM-2/S, weight losses were 11.99% and 11.58%. The higher weight loss observed in the case of slag-substituted mixtures might be attributed to the higher degree of dehydration and dehydroxylation due to formation of denser aluminosilicate gels. In this region, for CGM-3/S and CGM-3 mixtures, the peaks were detected at lower temperatures (405–410 °C) compared to other mixtures, which may be associated with the higher $Ca(OH)_2$ contents in these mixtures (Balachandra et al., 2021). Another reason for the peaks formed at higher temperatures, excluding CGM-3/S and CGM-3 mixtures, may be related to the dehydration of sodium carbonate, which is formed by the atmospheric carbonation of unreacted NaOH (Tchakouté et al., 2016). Considering all geopolymer mortars had more or less the same aluminosilicate networks, the weight losses due to dehydration and dehydroxylation of the aluminosilicate gel structure are expected to be similar, and the observed differences in Stage-II were thought to be due to NaOH reactivity. It is considered that the thermogravimetric response of CGM-3 and CGM-3/S mixtures designed only with NaOH and Ca(OH)₂ showed a high-efficiency reaction of NaOH, whereas the inclusion of Na_2SiO_3 is likely to reduce the reaction efficiency of NaOH, thereby leading to the presence of unreacted NaOH. This is also related to the efflorescence behavior of the CGM-3 and CGM-3/S mixtures, which exhibited almost no efflorescence products by consuming NaOH effectively.

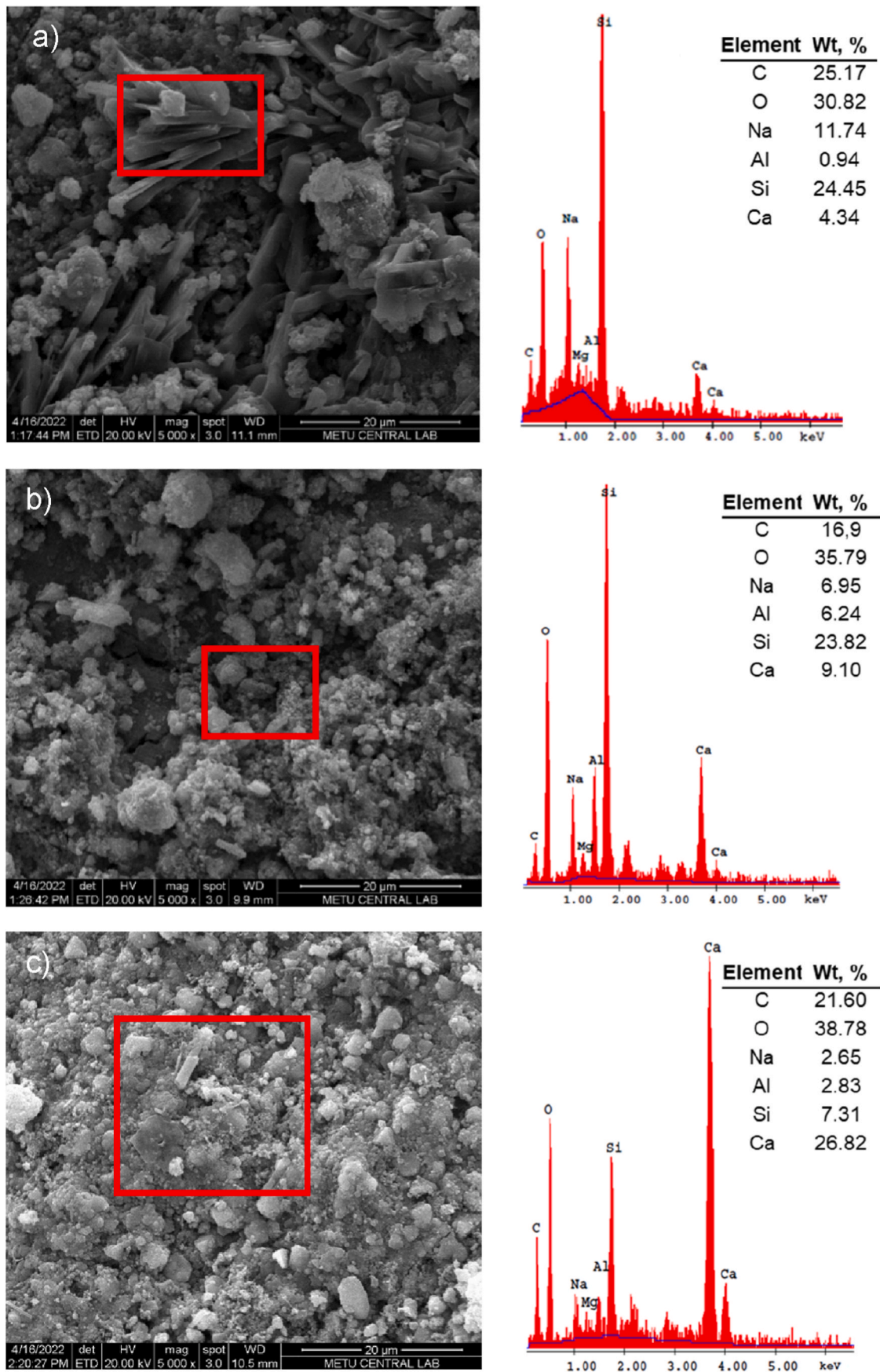In the temperature range between 600 and 800 °C indicated as Stage

Fig. 11. Representative SEM images and EDX analyses of CGM-2/S mixture from regions of (a) low, (b) moderate, and (c) high calcium.
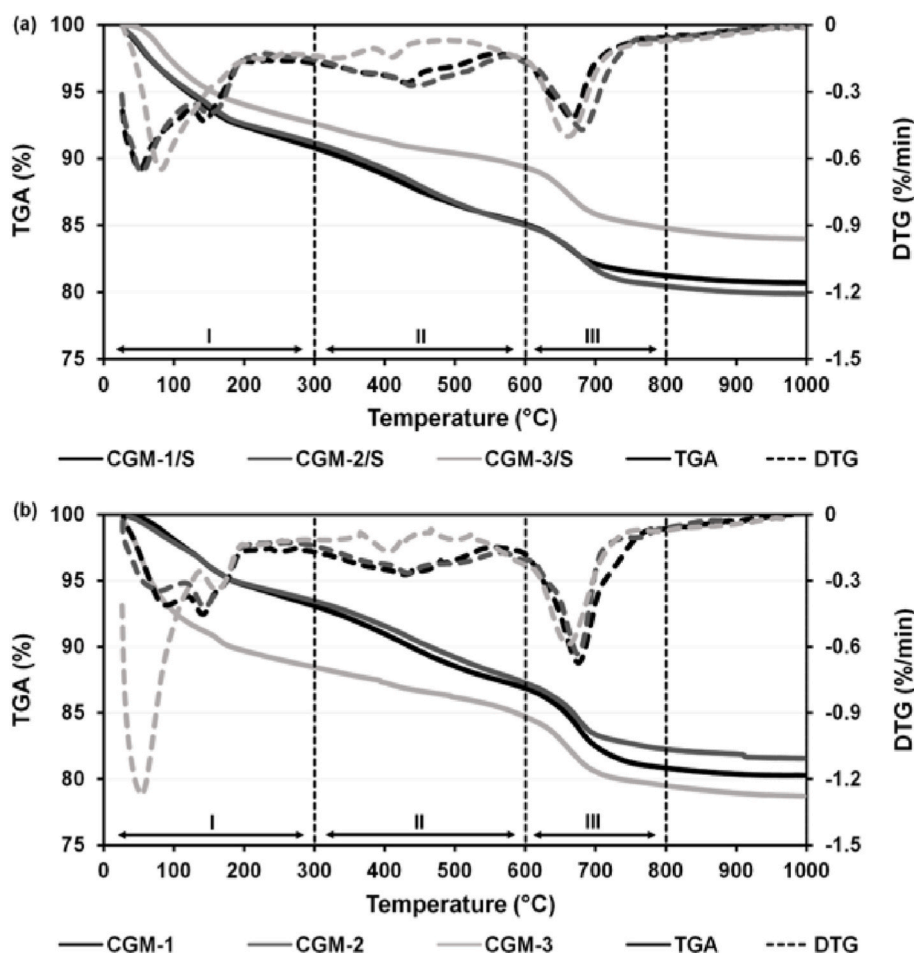
Fig. 12. Thermograms of the geopolymer mortars (a) slag-substituted mixtures, (b) completely CDW-based mixtures (straight and dashed lines represent the TGA and DTG plots).

III, the broad endothermic peaks around 670 °C were observed in all geopolymer mortars. This is associated with the decarbonation of calcium carbonate and sodium carbonate that are present in various crystalline forms (Lu et al., 2018). In this region, CGM-1/S and CGM-2/S showed the highest weight losses (approximately 17%) among the slag-substituted mixtures, while CGM-3 showed the highest weight loss (approximately 19%) among the completely CDW-based mixtures. Another notable point was that the mixtures without slag substitution showed more intense peaks than mixtures with slag substitution in this temperature range, which was related to possible consumption of free alkali ions in the system by the slag contributing to the formation of additional reaction products. In other words, in the presence of free alkalis in the system, alkalis tend to react with the atmospheric CO_2 to form alkali-carbonates, so, mixtures without slag substitution showed more intense peaks due to the availability of higher amounts of alkali-carbonates in their systems (Tchakouté et al., 2016).

3.5.3. Mercury intrusion porosimetry (MIP)

Results related to the MIP analyses including total porosity, pore size distribution and cumulative mercury intrusion volume were shown in Fig. 13. According to the results obtained, the total porosities of CGM-1/ S, CGM-2/S, and CGM-3/S were found to be 11.9%, 9.72%, and 11.5%, while the same results were 17.4%, 16.2, and 14.9%, for the CGM-1, CGM-2, and CGM-3 mixtures. The mixture with the lowest porosity was the CGM-2/S mixture, which also exhibited the highest compressive strength results after different ages. It is clear that the formation of compact and dense aluminosilicate gel structure and its homogeneous distribution in the matrices not only have a positive effect on the

compressive strength but also on the total porosity. This relationship observed between the compressive strength and total porosity results has also been similarly reported in the literature (Kusbiantoro et al., 2013). Considering the further microstructural improvements in the matrices with the use of slag, the total porosity results found for the slag-substituted CGM-1/S, CGM-2/S and CGM-3/S mixtures were expected (Li and Liu, 2007). It is known that the pores larger than 0.2 μm are available between the undissolved particles and aluminosilicate gels. The pores between 0.05 and 0.2 μm are the macropores that form in the initial stages of geopolymerization and turn into mesopores in the later stages, and the pores between 0.0036 and 0.05 μm are the mesopores, which are characteristic to the amorphous materials and present in the aluminosilicate gel network (Rodríguez et al., 2013). The lowest volume of mesopores was found in CGM-2/S mixture, followed by the CGM-1/S and CGM-3/S mixtures. Having less mesopores volume can be considered one of the influencing parameters for the achievement of a more compact and denser microstructure, as also reflected by the compressive strength results (Nikolić et al., 2017). It is notable that the presence of other pores (especially the larger ones [*i.e.*, macropores]) is also very effective on the compressive results. For example, although CGM-3 mixture showed the lowest volume of mesopores following the CGM-3/S mixture, this was not reflected in the compressive strength results, most probably due to the availability of larger pores and other related factors being involved.

Along with the relationship between the compressive strength and total porosity, results showed that there is also a close relationship between the water absorption and total porosity results. For instance, CGM-1 had the highest total porosity result and also the highest water
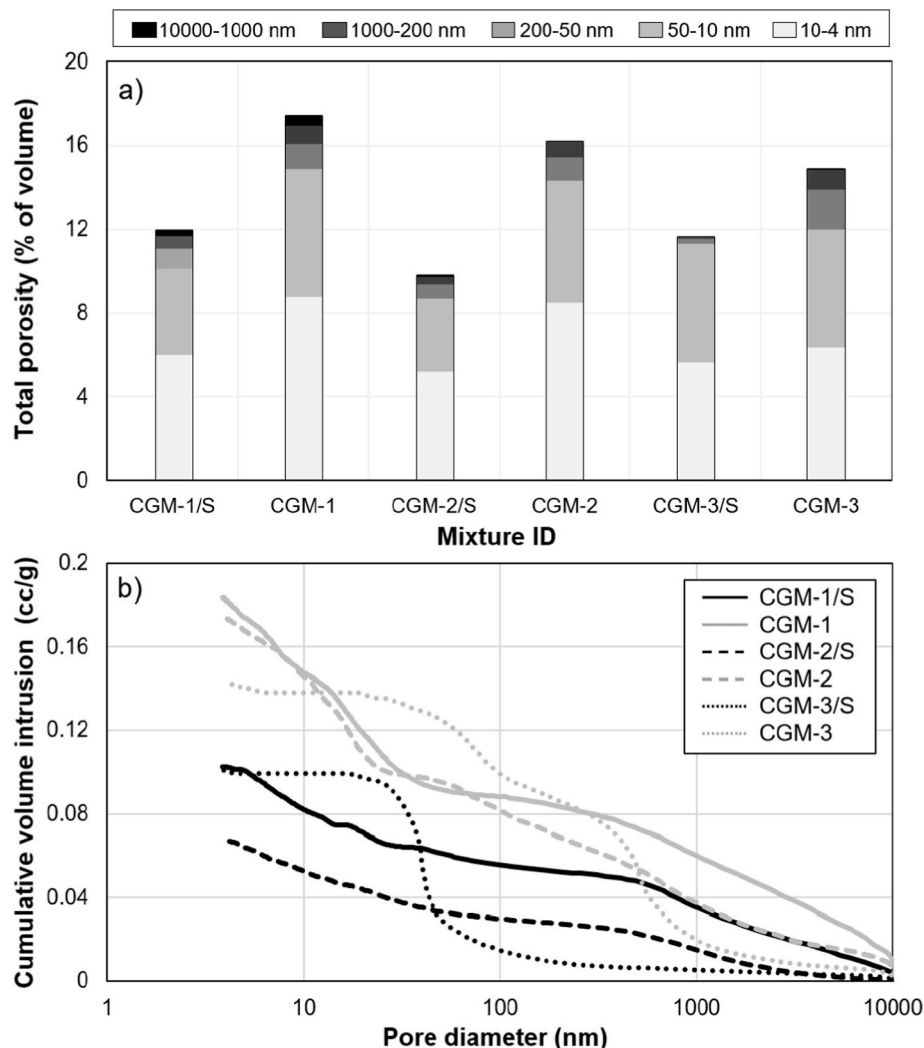
Fig. 13. MIP results of the CDW-based geopolymer mortars (a) total porosity with different-size pore distribution, (b) cumulative intruded pore volume.

absorption. Although the water absorption and the total porosity values were in parallel, there were deviations from this general trend. For instance, CGM-3/S mixture with the lowest water absorption did not have the lowest porosity (Figs. 8 and 13) which implied that together with the total porosity, the pore size distribution is decisive on the water absorption (Masi et al., 2014). It has been well reported that while pores greater than 50 nm are more effective on the permeability and strength properties of cement-based systems, pores smaller than 50 nm are more effective on drying shrinkage and creep (Mehta and Monteiro, 1993). Likewise, CGM-3/S mixture with the lowest water absorption had the lowest volume of pores (0.31%) with the size greater than 50 nm, showing the importance of pore size distribution on overall water absorption results. Similar results were also obtained for other mixtures. For example, CGM-2/S mixture with the lowest water absorption after CGM-3/S, had the lowest volume of pores (1.07%) with the size greater than 50 nm after CGM-3/S.

Considering the relationship between drying shrinkage and porosity, drying shrinkage is largely affected by the mesopore volume in the matrix, as stated in the literature (Collins and Sanjayan, 2000). A similar observation was made in this study that CGM-1 and CGM-2 mixtures, which exhibited the highest drying shrinkage after 90 d, had the highest mesopore volumes among other mixtures. A similar trend was also registered for the CGM-1/S and CMG-2/S mixtures that exhibited lower drying shrinkage results and lower mesopore volumes compared to CGM-1 and CMG-2 mixtures. No relationship could be established

between the drying shrinkage and mesopore volume of the CGM-3 and CGM-3/S mixtures as in other mixtures. This might be due to that the drying shrinkage of the mixtures is more affected by the use of Na_2SiO_3 rather than the effect of volume of the mesopores.

3.5.4. Nuclear magnetic resonance

NMR analysis enables the determination of the local chemical environments of NMR active nuclei through the signals and resonances that occur as a result of the interactions between the applied magnetic field and nuclei (Ozcelikci et al., 2022). For the characterization of the molecular framework of the geopolymeric gel structure, ^{29}Si MAS NMR and ^{27}Al MAS NMR analyses were carried out on the geopolymer mortars. While the nuclei of interest in cementitious composites and geopolymers in general are ^1H, ^{13}C, ^{17}O, ^{19}F, ^{23}Na, ^{25}Mg, ^{27}Al, ^{29}Si, ^{31}P, ^{33}S, ^{35}Cl, ^{39}K, and ^{43}Ca (Walkley and Provis, 2019), only ^{27}Al and ^{29}Si examinations were made for the current study to provide more valuable insight into the formations of geopolymeric gel structure. In ^{29}Si MAS NMR analysis, the bond structures are defined as $Q^n(mAl)$, while the Q indicator represents the tetrahedral coordination of Si atoms, the n indicator represents the number of bonds of Si to other atoms via oxygen, and the m indicator represents neighboring Al atoms. In previous literature studies, which examined the gel structure of the geopolymers through NMR analysis, it has been reported that silicon and aluminum sites are in tetrahedral coordination and the silicate coordinate number (n) of geopolymeric gels is 4 (Barbosa et al., 2000). In ^{27}Al MAS NMR analysis,

q^n indicator is generally used to define tetrahedral Al species, where q indicates Al coordination linked to n tetrahedral silicon with the oxygen bridges (Walkley and Provis, 2019).

The results of ^{29}Si MAS NMR and ^{27}Al MAS NMR analyses obtained from the CDW-based geopolymer mortars are presented in Fig. 14. According to the results presented in Fig. 14-a, the chemical shift values were found to range from −80.023 to −98.118 ppm with a broad resonance. Literature studies have reported that well-cured geopolymers exhibit a broad resonance behavior in the range of −85 to −95 ppm and the sharp resonances between −80 and −100 ppm indicate the presence of unreacted silicate oligomers that are not bound to a gel structure (Provis and Van Deventer, 2013). Based on this, CDW-based geopolymer mortars produced herein confirms the formation of typical geopolymer gel structure as mentioned in the literature. Comparing the ^{29}Si chemical shift analysis of aluminosilicate-based inorganic materials in literature (MacKenzie and Smith, 2002), CGM-1/S and CGM-1 samples were found to have $Q^4(2Al)$ site due to the presence of the centered shift at about −98.118 and −97.191 ppm. In the CGM-2/S mixture, the chemical shift was centered at about −86.368 ppm and was corresponding to the $Q^4(3Al)$ site. In accordance with the chemical shift values, in CGM-2, CGM-3/S, and CGM-3 mixtures, $Q^4(1Al)$, $Q^4(4Al)$, $Q^4(4Al)$ sites were observed. According to the structural orders of the CDW-based geopolymer mortars, all mixtures exhibited typical tetrahedral silicate centers bonded by several numbers of aluminum atoms. These findings indicated that geopolymers contain 3D cross-linked sites, which correspond with the highly polymerised structural aluminosilicate framework (Lecomte et al., 2006). It was also observed that while the slag substitution did not cause a significant change in the structural framework developments, the addition of Na_2SiO_3 plays a more essential role in the development of the different structural orders than slag substitution.

In accordance with the results of ^{27}Al MAS NMR analysis results, a narrow resonance centered in the range of 169.015–174.640 ppm, 9.746–14.642 ppm, and −53.193 to −49.309 ppm, together with the broad resonance centered in the range of 58.328–60.605 ppm were observed for all CDW-based geopolymer mortars. ^{27}Al MAS NMR spectra showed that resonances at about 9.746–14.642 ppm indicated a lower amount of octahedrally coordinated Al in the framework of gel structure. The broad and larger resonances at around 58.328–60.605 ppm indicated that major content was tetrahedrally coordinated Al in the related structural order (Lecomte et al., 2006). The major difference in

Al coordination among CDW-based geopolymer mortar samples is the geopolymerization kinetics. As the reactions continue, the wider resonances become sharper by showing a higher structural order, as in zeolite-type structures (Provis and Van Deventer, 2013). It was reported that as a result of the geopolymerization reactions of unreacted fly ash, the wide peak characterized by NMR MAS became sharper and had a higher structural order indicating the presence of high contents of crystalline phases (Wan et al., 2017). This situation became more evident, especially in the case of CGM-2/S sample, which showed the highest compressive strength, while the wider resonance of CGM-3 compared to other samples may be associated with the lowest strength results recorded.

3.6. Interrelationship among the experimental results

The interrelationship among the selected experimental results, which were quantitively measurable, was presented in Fig. 15. Although comparative discussions were made in the related sections, results were collected and presented altogether in Fig. 15 for clarity and easier comparison. According to Fig. 15, irrespective of the mixture composition, a close relationship between the porosity and water absorption results was noted. The relationship between the porosity and drying shrinkage was closely related to the mesopore volume in the matrices and direct proportional relationship was observed for all the mixtures except for CGM-3 and CGM-3/S which lacked Na_2SiO_3, the alkaline activator with the greatest effect on drying shrinkage and did not exhibit such a relationship. Compressive strength results were found to be inversely proportional to the other three parameters (total porosity, water absorption, and drying shrinkage). The increments in these three parameters, which had almost linear relationships between themselves, mainly caused decrements in the compressive strength results.

3.7. Sustainability analysis

Development of eco-friendly construction materials to ensure long-term sustainability is of major importance. Geopolymer binders are being developed as an alternative to the traditional Portland cement. Assessment of the materials sustainability and greenness of existing geopolymer binders must be carefully considered. Material Sustainability Index (MSI) has been developed to quantify the environmental
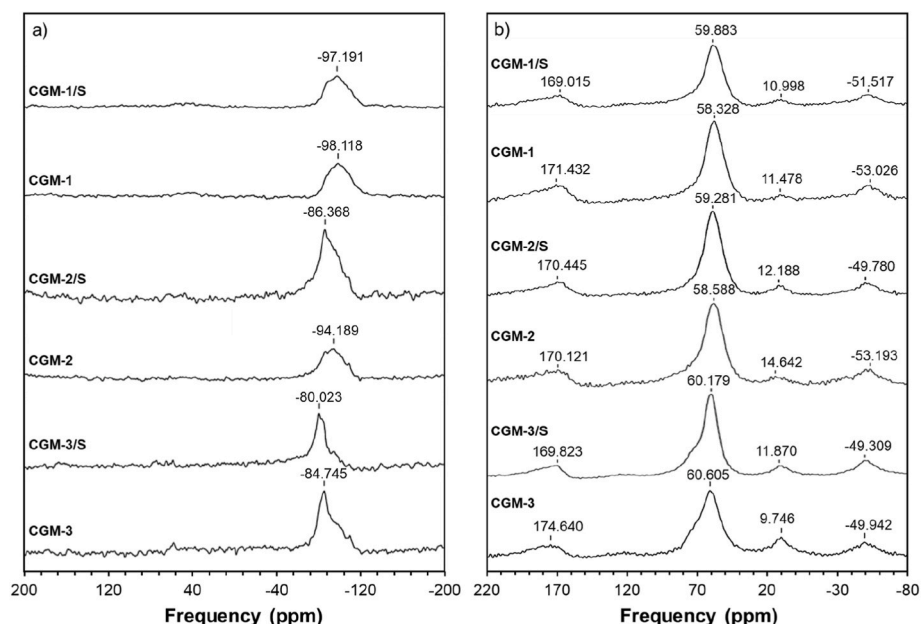

Fig. 14. (a) ^{29}Si MAS NMR, (b) ^{27}Al MAS NMR spectra of CDW-based geopolymer mortars.
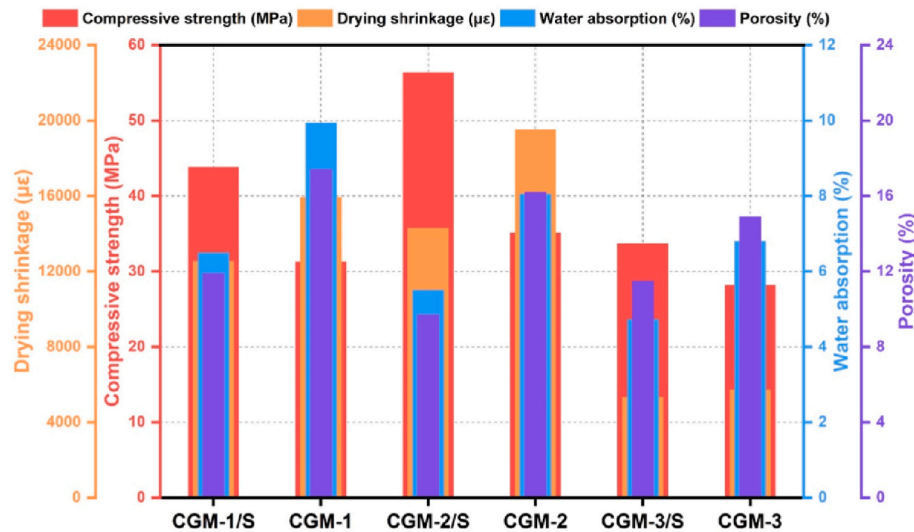
Fig. 15. Interrelationship among the experimental results.

effect and the material sustainability of the newly developed alternative materials (Keoleian et al., 2005). The MSI evaluation is very useful in investigating the environmental impacts of the products, their manufacturing and processing, as well as in determining the carbon and energy footprints. Material sustainability was evaluated by using MSI for the components of the mixtures used herein. Reliable life cycle inventory data for all the components of the mixtures was collected from the literature or database. The life cycle inventory data of the materials used in this study were listed in Table 4. All the data presented in Table 4 represents the values related to the production of the materials, and the data originated by transportation were not taken into account. Data related to CDW-based materials were calculated based on the time and energy consumed by the laboratory jaw crusher/ball mill and the CO_2 emissions generated during the acquirement of consumed energy, similar to the work of Mahmoodi et al. (2020).

In Fig. 16, embodied energy and global warming impact assessments of the geopolymer mortar mixtures designed in this study and traditional Portland cement mortars (with 28 d compressive strength of 32.5 MPa) were presented. It can be clearly seen that the CO_2 emissions calculated for CDW-based geopolymer mortar mixtures are largely dependent on the alkaline activator usage. CDW-based geopolymer mortars exhibited

quite low CO_2 emissions compared to traditional Portland cement-based counterparts. This was mainly due to the absence of Portland cement in the geopolymer mixtures. Geopolymer mixtures had lower energy consumption levels. Such energy consumption of geopolymer mixtures largely arises from the use of alkaline activators in their production. Together with the sustainability analysis, the efficiency values were calculated by dividing the energy consumption and global warming intensity values with the compressive strength results. According to the red line indicator based on MJ/m^3.MPa (Fig. 16-a) and kg CO_2-eq/m^3. MPa values (Fig. 16-b), it was observed that CDW-based geopolymer mortars, especially CGM-2/S being in the first place, had very high efficiency in terms of energy consumption and CO_2 emissions. CDW-based geopolymer mortars were found to be highly advantageous in terms of their environmental friendliness within the context of developing construction materials alternative to those produced by the ordinary Portland cement.

4. Conclusions

This paper investigated the development and characterization of ambient-cured mortars with mixed CDW-based geopolymer binders and untreated FRCA. Reaching reasonably high compressive strength levels to suit the developed mortars for future designs of completely CDW-based structural geopolymer concretes and elements was aimed alongside with revealing durability-related parameters (*i.e.*, drying shrinkage, water absorption, and efflorescence) critical for the long-term performance. Detailed microstructural characterization and material sustainability analysis were also performed. Following conclusions were drawn from the experimental work undertaken:

- Depending on the mixture design, it is possible to achieve 28 d compressive strength exceeding 30 and 50 MPa, with the entirely CDW-based mortars and with the 20% slag replacement of CDW-based precursors, which are promising strength levels that can be scaled up to have entirely CDW-based structural concretes and elements. Utilization of Na_2SiO_3 and slag had positive effect on the compressive strength. A similar effect was also observed at later ages for the mixtures incorporated with $Ca(OH)_2$.
- Drying shrinkage strains were the highest for mixtures produced with Na_2SiO_3 while for those incorporated with slag, early age drying shrinkage was restricted. Since the mixtures were manufactured with a constant and reasonably low amount of FRCA, the drying shrinkage strains of the CDW-based mortars were slightly higher than and/or comparable to the cementitious/geopolymer mortars based on

Table 4
Life cycle inventories of the materials.

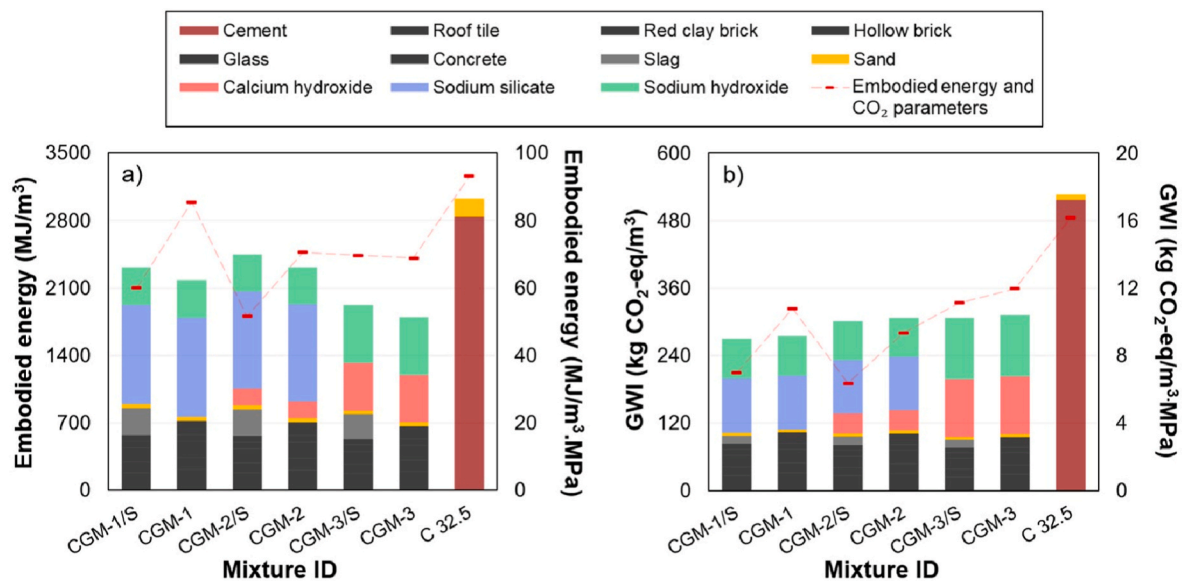| Material	Reference	Embodied energy (MJ/t)	Global warming intensity (kg.CO_2-eq/t)
Roof tile	–	675	96.9
Red clay brick	–	675	96.9
Hollow brick	–	675	96.9
Glass	–	675	96.9
Concrete	–	675	96.9
Recycled aggregate	–	112.5	13.84
Normal aggregate	Nisbet et al. (2000)	120	6.20
Portland cement	Barcelo et al. (2014)	5500	1000
Slag	Yu et al. (2021)	1300	70
Na_2SiO_3	Fawer et al. (1999)	4600	430
NaOH	Mahmoodi et al. (2020)	3500	633
$Ca(OH)_2$	Gutiérrez et al. (2012)	4464	938
Water	Jones et al. (2011)	–	–

Fig. 16. Results of sustainability analysis, (a) embodied energy and (b) global warming impact for CDW-based geopolymer mortars and ordinary Portland cement mortars.

mainstream precursors with low content of aggregates. It was inferred that with small modifications in the FRCA gradation and content it is possible to reach much lower drying shrinkage strains.

- Slag substitution led to denser and more compact matrices thereby lowering the water absorption, while the use of Na_2SiO_3 negatively affected this parameter. This was mainly attributed to the formation of randomly oriented map-type microcracks due to the higher drying shrinkage in the presence of Na_2SiO_3. Nevertheless, the level of water absorption was still at acceptable levels compared to literature studies.

- Although the efflorescence formation was observed at various degrees in some mixtures; its effect on the compressive strength and other durability-related parameters was limited. Taking the mixture with the highest compressive strength as an example, which had very limited efflorescence, it seems very likely to eliminate the efflorescence formation almost completely via further tailoring of the mixture designs.

- SEM/EDX analysis revealed that NASH gel formation was observed mostly in the regions where the amount of calcium is low, whereas hybrid NASH and calcium-based gels such as CSH, CASH and C(N) ASH were present together in the regions where the amount of calcium is high, leading to a denser and more compact matrix. In TGA/DTG analysis, slag-substitution was the most influential parameter for the variations of weight changes/endothermic peaks caused by evaporation of loosely bound water, dehydration and dehydroxylation of the aluminosilicate gel structure and the decarbonation of calcium carbonate and sodium carbonate. MIP analysis revealed that lower pore volume led to the realization of higher compressive strength results. The water absorption was mainly governed by the pores with the size greater than 50 nm, while the extent of drying shrinkage of the mixtures produced with Na_2SiO_3 was mainly driven by the pores with the size smaller than 50 nm. NMR analyses revealed that CDW-based geopolymer mortars were with 3D crosslinked sites and the usage of Na_2SiO_3 was one of the key parameters determining the structural orders.

- The MSI evaluation proved that CDW-based geopolymers were significantly advantageous over the ordinary Portland cement-based mortars in terms of CO_2 emission and energy consumption values. This outcome was clearer in the case of CGM-2/S mixture, which also exhibited the highest compressive strength.

CRediT authorship contribution statement

Emircan Ozcelikci: Investigation, Methodology, Writing – original draft. **Anil Kul:** Investigation, Methodology, Writing – original draft. **Muhammed Faruk Gunal:** Investigation, Methodology, Writing – original draft. **Behlul Furkan Ozel:** Investigation, Methodology, Writing – original draft. **Gurkan Yildirim:** Funding acquisition, Data curation, Investigation, Methodology, Conceptualization, Writing – original draft, Writing – review & editing. **Ashraf Ashour:** Funding acquisition, Supervision, Writing – review & editing. **Mustafa Sahmaran:** Writing – review & editing.

Declaration of competing interest

The authors declare that they have no known competing financial interests or personal relationships that could have appeared to influence the work reported in this paper.

Data availability

Data will be made available on request.

References

Adesanya, E., Ohenoja, K., Luukkonen, T., Kinnunen, P., Illikainen, M., 2018. One-part geopolymer cement from slag and pretreated paper sludge. J. Clean. Prod. 185, 168–175. https://doi.org/10.1016/j.jclepro.2018.03.007.

Alhawat, M., Ashour, A., Yildirim, G., Aldemir, A., Sahmaran, M., 2022. Properties of geopolymers sourced from construction and demolition waste: a review. J. Build. Eng. 50, 104104.

Alonso, S., Palomo, A., 2001. Alkaline activation of metakaolin and calcium hydroxide mixtures: influence of temperature, activator concentration and solids ratio. Mater. Lett. 47 (1–2), 55–62. https://doi.org/10.1016/S0167-577X(00)00212-3.

Alventosa, K.M., White, C.E., 2021. The effects of calcium hydroxide and activator chemistry on alkali-activated metakaolin pastes. Cement Concr. Res. 145, 106453 https://doi.org/10.1016/j.cemconres.2021.106453.

ASTM C109, 2020. Standard Test Method for Compressive Strength of Hydraulic Cement Mortars (Using 2-in. Or [50-mm] Cube Specimens). ASTM International, West Conshohocken, PA.

ASTM C596, 2018. Standard Test Method for Drying Shrinkage of Mortar Containing Hydraulic Cement. ASTM International, West Conshohocken, PA.

ASTM C642, 2013. Standard Test Method for Density, Absorption, and Voids in Hardened Concrete. ASTM International, West Conshohocken, PA.

Atiş, C.D., Bilim, C., Çelik, O., Karahan, O., 2009. Influence of activator on the strength and drying shrinkage of alkali-activated slag mortar. Construct. Build. Mater. 23 (1), 548–555. https://doi.org/10.1016/j.conbuildmat.2007.10.011.

Bădănoiu, A.I., Al-Saadi, T.H.A., Voicu, G., 2015. Synthesis and properties of new materials produced by alkaline activation of glass cullet and red mud. Int. J. Miner. Process. 135, 1–10. https://doi.org/10.1016/j.minpro.2014.12.002.

Balachandra, A.M., Abdol, N., Darsanasiri, A.G.N.D., Zhu, K., Soroushian, P., Mason, H. E., 2021. Landfilled coal ash for carbon dioxide capture and its potential as a geopolymer binder for hazardous waste remediation. J. Environ. Chem. Eng. 9 (4), 105385 https://doi.org/10.1016/j.jece.2021.105385.

Barbosa, V.F., MacKenzie, K.J., Thaumaturgo, C., 2000. Synthesis and characterisation of materials based on inorganic polymers of alumina and silica: sodium polysialate polymers. Int. J. Inorg. Mater. 2 (4), 309–317. https://doi.org/10.1016/S1466-6049 (00)00041-6.

Barcelo, L., Kline, J., Walenta, G., Gartner, E., 2014. Cement and carbon emissions. Mater. Struct. 47 (6), 1055–1065. https://doi.org/10.1617/s11527-013-0114-5.

Baronio, G., Binda, L., 1997. Study of the pozzolanicity of some bricks and clays. Construct. Build. Mater. 11 (1), 41–46. https://doi.org/10.1016/S0950-0618(96) 00032-3.

Bassani, M., Tefa, L., Russo, A., Palmero, P., 2019. Alkali-activation of recycled construction and demolition waste aggregate with no added binder. Construct. Build. Mater. 205, 398–413. https://doi.org/10.1016/j.conbuildmat.2019.02.031.

Bellum, R.R., Muniraj, K., Madduru, S.R.C., 2020. Influence of slag on mechanical and durability properties of fly ash-based geopolymer concrete. J. Korean Ceram. Soc. 57, 530–545. https://doi.org/10.1007/s43207-020-00056-7.

Collins, F., Sanjayan, J.G., 2000. Effect of pore size distribution on drying shrinking of alkali-activated slag concrete. Cement Concr. Res. 30 (9), 1401–1406. https://doi.org/10.1016/S0008-8846(00)00327-6.

Dadsetan, S., Siad, H., Lachemi, M., Sahmaran, M., 2019. Construction and demolition waste in geopolymer concrete technology: a review. Mag. Concr. Res. 71 (23), 1232–1252. https://doi.org/10.1680/jmacr.18.00307.

Davidovits, J., 2008. Geopolymer Chemistry and Applications, second ed. Geopolymer Institute, Saint-Quentin, France.

Deb, P.S., Nath, P., Sarker, P.K., 2015. Drying shrinkage of slag blended fly ash geopolymer concrete cured at room temperature. Procedia Eng. 125, 594–600. https://doi.org/10.1016/j.proeng.2015.11.066.

Duxson, P.S.W.M., Mallicoat, S.W., Lukey, G.C., Kriven, W.M., van Deventer, J.S., 2007. The effect of alkali and Si/Al ratio on the development of mechanical properties of metakaolin-based geopolymers. Colloids Surf. A Physicochem. Eng. Asp. 292 (1), 8–20. https://doi.org/10.1016/j.colsurfa.2006.05.044.

Escalante-Garcia, J.I., Fuentes, A.F., Gorokhovsky, A., Fraire-Luna, P.E., Mendoza-Suarez, G., 2003. Hydration products and reactivity of blast-furnace slag activated by various alkalis. J. Am. Ceram. Soc. 86 (12), 2148–2153. https://doi.org/10.1111/j.1151-2916.2003.tb03623.x.

European Commission, 2019. Construction and Demolition Waste (CDW).

Fawer, M., Concannon, M., Rieber, W., 1999. Life cycle inventories for the production of sodium silicates. Int. J. LCA. 4 (4), 207–212. https://doi.org/10.1007/BF02979498.

Frias, M., Vigil de la Villa, R., Martinez-Ramirez, S., Fernandez-Carrasco, L., Villar-Cocina, E., Garcia-Gimenez, R., 2020. Multi-Technique characterization of a fine fraction of CDW and assessment of reactivity in a CDW/Lime system. Minerals 10 (7), 590. https://doi.org/10.3390/min10070590.

Garcia-Lodeiro, I., Palomo, A., Fernández-Jimenez, A., Macphee, D.E., 2011. Compatibility studies between NASH and CASH gels. Study in the ternary diagram Na$_2$O–CaO–Al$_2$O$_3$–SiO$_2$–H$_2$O. Cement Concr. Res. 41 (9), 923–931. https://doi.org/10.1016/j.cemconres.2011.05.006.

Gutierrez, A.S., Van Caneghem, J., Martinez, J.B.C., Vandecasteele, C., 2012. Evaluation of the environmental performance of lime production in Cuba. J. Clean. Prod. 31, 126–136. https://doi.org/10.1016/j.jclepro.2012.02.035.

Hager, I., Sitarz, M., Mroz, K., 2021. Fly-ash based geopolymer mortar for high-temperature application–Effect of slag addition. J. Clean. Prod. 316, 128168 https://doi.org/10.1016/j.jclepro.2021.128168.

Ismail, I., Bernal, S.A., Provis, J.L., San Nicolas, R., Hamdan, S., van Deventer, J.S., 2014. Modification of phase evolution in alkali-activated blast furnace slag by the incorporation of fly ash. Cem. Concr. Compos. 45, 125–135. https://doi.org/10.1016/j.cemconcomp.2013.09.006.

Jones, R., McCarthy, M., Newlands, M., 2011. Fly ash route to low embodied CO2 and implications for concrete construction. In: World of Coal Ash Conference. Denver, Co, USA.

Kaze, C.R., Lemougna, P.N., Alomayri, T., Assaedi, H., Adesina, A., Das, S.K., Lecomte-Nana, G.L., Kamseu, E., Melo, U.C., Leonelli, C., 2021. Characterization and performance evaluation of laterite based geopolymer binder cured at different temperatures. Construct. Build. Mater. 270, 121443 https://doi.org/10.1016/j.conbuildmat.2020.121443.

Keoleian, G., Kendall, A.M., Lepech, M.D., Li, V.C., 2005. Guiding the Design and Application of New Materials for Enhancing Sustainability Performance: Framework and Infrastructure Application. MRS Online Proceedings Library (OPL), p. 895.

Komnitsas, K., Zaharaki, D., Vlachou, A., Bartzas, G., Galetakis, M., 2015. Effect of synthesis parameters on the quality of construction and demolition wastes (CDW) geopolymers. Adv. Powder Technol. 26, 368–376. https://doi.org/10.1016/j.apt.2014.11.012.

Kusbiantoro, A., Ibrahim, M.S., Muthusamy, K., Alias, A., 2013. Development of sucrose and citric acid as the natural based admixture for fly ash based geopolymer. Proc. Environ. Sci. 17, 596–602. https://doi.org/10.1016/j.proenv.2013.02.075.

Lecomte, I., Henrist, C., Liegeois, M., Maseri, F., Rulmont, A., Cloots, R., 2006. (Micro)-structural comparison between geopolymers, alkali-activated slag cement and Portland cement. J. Eur. Ceram. Soc. 26 (16), 3789–3797. https://doi.org/10.1016/j.jeurceramsoc.2005.12.021.

Li, Z., Liu, S., 2007. Influence of slag as additive on compressive strength of fly ash-based geopolymer. J. Mater. Civ. Eng. 19 (6), 470–474. https://doi.org/10.1061/(ASCE) 0899-1561 (2007)19:6(470).

Lloyd, R.R., Provis, J.L., Van Deventer, J.S., 2010. Pore solution composition and alkali diffusion in inorganic polymer cement. Cement Concr. Res. 40 (9), 1386–1392. https://doi.org/10.1016/j.cemconres.2010.04.008.

Lu, B., Shi, C., Zhang, J., Wang, J., 2018. Effects of carbonated hardened cement paste powder on hydration and microstructure of Portland cement. Construct. Build. Mater. 186, 699–708. https://doi.org/10.1016/j.conbuildmat.2018.07.159.

MacKenzie, K.J., Smith, M.E., 2002. Multinuclear Solid-State Nuclear Magnetic Resonance of Inorganic Materials. Elsevier.

Maghsoodloorad, H., Allahverdi, A., 2016. Efflorescence formation and control in alkali-activated phosphorus slag cement. Int. J. Civ. Eng. 14 (6), 425–438. https://doi.org/10.1007/s40999-016-0027-0.

Mahmoodi, O., Siad, H., Lachemi, M., Dadsetan, S., Sahmaran, M., 2020. Optimization of brick waste-based geopolymer binders at ambient temperature and pre-targeted chemical parameters. J. Clean. Prod., 122285 https://doi.org/10.1016/j.jclepro.2020.122285.

Marjanovic, N., Komljenović, M., Baščarević, Z., Nikolic, V., Petrovic, R., 2015. Physical–mechanical and microstructural properties of alkali-activated fly ash–blast furnace slag blends. Ceram. Int. 41 (1), 1421–1435. https://doi.org/10.1016/j.ceramint.2014.09.075.

Masi, G., Rickard, W.D., Vickers, L., Bignozzi, M.C., Van Riessen, A., 2014. A comparison between different foaming methods for the synthesis of light weight geopolymers. Ceram. Int. 40 (9), 13891–13902. https://doi.org/10.1016/j.ceramint.2014.05.108.

Matalkah, F., Salem, T., Shaafaey, M., Soroushian, P., 2019. Drying shrinkage of alkali activated binders cured at room temperature. Construct. Build. Mater. 201, 563–570. https://doi.org/10.1016/j.conbuildmat.2018.12.223.

Mehta, P.K., Monteiro, P.J.M., 1993. Concrete Structure, Properties and Materials, 2. Prentice Hall, New Jersey.

Mobasheri, F., Shirzadi Javid, A.A., Mirvalad, S., Azizi, S., Mowlaei, R., 2022. Durability and mechanical properties of pumice-based geopolymers: a sustainable material for future. J. Sci. Technol. Trans. Civ. Eng. 46 (1), 223–235. https://doi.org/10.1007/s40996-021-00651-6.

Moreno-Maroto, J.M., Delgado-Plana, P., Cabezas-Rodriguez, R., de Gutierrez, R.M., Eliche-Quesada, D., Perez-Villarejo, L., Galan-Arboledas, R.J., Bueno, S., 2022. Alkaline activation of high-crystalline low-Al2O3 Construction and Demolition Wastes to obtain geopolymers. J. Clean. Prod. 330, 129770 https://doi.org/10.1016/j.jclepro.2021.129770.

Myers, R.J., Provis, J.L., Lothenbach, B., 2015. Composition–solubility–structure relationships in calcium (alkali) aluminosilicate hydrate (C-(N, K-) ASH). Dalton Trans. 44 (30), 13530–13544. https://doi.org/10.1039/C5DT01124H.

Nath, P., Sarker, P.K., 2014. Effect of GGBFS on setting, workability and early strength properties of fly ash geopolymer concrete cured in ambient condition. Construct. Build. Mater. 66, 163–171. https://doi.org/10.1016/j.conbuildmat.2014.05.080.

Nergis, D.D.B., Abdullah, M.M.A.B., Sandu, A.V., Vizureanu, P., 2020. XRD and TG-DTA study of new alkali activated materials based on fly ash with sand and glass powder. Materials 13 (2), 343. https://doi.org/10.3390/ma13020343.

Nguyen, T.K.L., Ngo, H.H., Guo, W., Nguyen, T.L.H., Chang, S.W., Nguyen, D.D., Varjani, S., Lei, Z., Deng, L., 2021. Environmental impacts and greenhouse gas emissions assessment for energy recovery and material recycle of the wastewater treatment plant. Sci. Total Environ. 784, 147135 https://doi.org/10.1016/j.scitotenv.2021.147135.

Nikolic, V., Komljenovic, M., Dzunuzovic, N., Ivanovic, T., Miladinovic, Z., 2017. Immobilization of hexavalent chromium by fly ash-based geopolymers. Compos. B Eng. 112, 213–223. https://doi.org/10.1016/j.compositesb.2016.12.024.

Nisbet, M.A., VanGeem, M.G., Gajda, J., Marceau, M., 2000. Environmental Life Cycle Inventory of Portland Cement Concrete. PCA R&D Serial, 2137a.

Oikonomou, N.D., 2005. Recycled concrete aggregates. Cem. Concr. Compos. 27 (2), 315–318. https://doi.org/10.1016/j.cemconcomp.2004.02.020.

Ozcelikci, E., Ilcan, H., Yildirim, G., Sahmaran, M., 2022. Nanoscale characterization of cementitious composites. In: Şahmaran, M., Shaikh, F., Yildirim, G. (Eds.), Recent Advances in Nano-Tailored Multi-Functional Cementitious Composites, pp. 375–406. https://doi.org/10.1016/B978-0-323-85229-6.00006-8.

Palomo, A., Grutzeck, M.W., Blanco, M.T., 1999. Alkali-activated fly ashes: a cement for the future. Cement Concr. Res. 29 (8), 1323–1329. https://doi.org/10.1016/S0008-8846(98)00243-9.

Pawluczuk, E., Kalinowska-Wichrowska, K., Jimenez, J.R., Fernandez-Rodriguez, J.M., Suescum-Morales, D., 2021. Geopolymer concrete with treated recycled aggregates: macro and microstructural behavior. J. Build. Eng. 44, 103317 https://doi.org/10.1016/j.jobe.2021.103317.

Provis, J.L., Lukey, G.C., van Deventer, J.S., 2005. Do geopolymers actually contain nanocrystalline zeolites? A reexamination of existing results. Chem. Mater. 17 (12), 3075–3085. https://doi.org/10.1021/cm050230i.

Provis, J.L., Van Deventer, J.S., 2013. Alkali Activated Materials: State-Of-The-Art Report. In: RILEM TC 224-AAM, 13. Springer Science & Business Media.

Pu, S., Zhu, Z., Song, W., Huo, W., Zhang, J., 2021. Mechanical and microscopic properties of fly ash phosphoric acid-based geopolymer paste: a comprehensive study. Construct. Build. Mater. 299, 123947 https://doi.org/10.1016/j.conbuildmat.2021.123947.

Rahman, A., Rasul, M.G., Khan, M.M.K., Sharma, S., 2015. Recent development on the uses of alternative fuels in cement manufacturing process. Fuel 145, 84–99. https://doi.org/10.1016/j.fuel.2014.12.029.

Rashidian-Dezfouli, H., Rangaraju, P.R., 2017. Comparison of strength and durability characteristics of a geopolymer produced from fly ash, ground glass fiber and glass powder. Mater. Construcción 67 (328). https://doi.org/10.3989/mc.2017.05416 e136-e136.

Robayo-Salazar, R.A., Rivera, J.F., de Gutierrez, R.M., 2017. Alkali-activated building materials made with recycled construction and demolition wastes. Construct. Build. Mater. 149, 130–138. https://doi.org/10.1016/j.conbuildmat.2017.05.122.

Robayo-Salazar, R.A., Valencia-Saavedra, W., Mejía de Gutierrez, R., 2020. Construction and demolition waste (CDW) recycling—As both binder and aggregates—In alkali-activated materials: a novel re-use concept. Sustainability 12 (14), 5775. https://doi.org/10.3390/su12145775.

Rodriguez, E.D., Bernal, S.A., Provis, J.L., Paya, J., Monzo, J.M., Borrachero, M.V., 2013. Effect of nanosilica-based activators on the performance of an alkali-activated fly ash binder. Cem. Concr. Compos. 35 (1), 1–11. https://doi.org/10.1016/j.cemconcomp.2012.08.025.

Sharma, A., Singh, P., Kapoor, K., 2022. Utilization of recycled fine powder as an activator in fly ash based geopolymer mortar. Construct. Build. Mater. 323, 126581 https://doi.org/10.1016/j.conbuildmat.2022.126581.

Sivasakthi, M., Jeyalakshmi, R., 2021. Effect of change in the silica modulus of sodium silicate solution on the microstructure of fly ash geopolymers. J. Build. Eng. 44, 102939 https://doi.org/10.1016/j.jobe.2021.102939.

Solyman, M., 2005. Classification of Recycled Sands and Their Applications as Fine Aggregates for Concrete and Bituminous Mixtures. Doctoral Dissertation. Fachbereich Bauingenieurwesen der Universitat Kassel, Kassel.

Taghvayi, H., Behfarnia, K., Khalili, M., 2018. The effect of alkali concentration and sodium silicate modulus on the properties of alkali-activated slag concrete. J. Adv. Concr. Technol. 16 (7), 293–305. https://doi.org/10.3151/jact.16.293.

Tan, J., Cai, J., Li, J., 2022a. Recycling of unseparated construction and demolition waste (UCDW) through geopolymer technology. Construct. Build. Mater. 341, 127771 https://doi.org/10.1016/j.conbuildmat.2022.127771.

Tan, J., Cizer, O., De Vlieger, J., Dan, H., Li, J., 2022b. Impacts of milling duration on construction and demolition waste (CDW) based precursor and resulting geopolymer: reactivity, geopolymerization and sustainability. Resour. Conserv. Recycl. 184, 106433 https://doi.org/10.1016/j.resconrec.2022.106433.

Tan, J., Cizer, O., Vandevyvere, B., De Vlieger, J., Dan, H., Li, J., 2022c. Efflorescence mitigation in construction and demolition waste (CDW) based geopolymer. J. Build. Eng. 58, 105001 https://doi.org/10.1016/j.jobe.2022.105001.

Tang, D., Yang, C., Li, X., Zhu, X., Yang, K., Yu, L., 2021. Mitigation of efflorescence of alkali-activated slag mortars by incorporating calcium hydroxide. Construct. Build. Mater. 298, 123873 https://doi.org/10.1016/j.conbuildmat.2021.123873.

Tchakouté, H.K., Ruscher, C.H., Kong, S., Ranjbar, N., 2016. Synthesis of sodium waterglass from white rice husk ash as an activator to produce metakaolin-based geopolymer cements. J. Build. Eng. 6, 252–261. https://doi.org/10.1016/j.jobe.2016.04.007.

Temuujin, J.V., Van Riessen, A., Williams, R., 2009. Influence of calcium compounds on the mechanical properties of fly ash geopolymer pastes. J. Hazard Mater. 167 (1–3), 82–88. https://doi.org/10.1016/j.jhazmat.2008.12.121.

Thomas, J.J., Allen, A.J., Jennings, H.M., 2012. Density and water content of nanoscale solid C–S–H formed in alkali-activated slag (AAS) paste and implications for chemical shrinkage. Cement Concr. Res. 42 (2), 377–383. https://doi.org/10.1016/j.cemconres.2011.11.003.

Tuyan, M., Andiç-Çakir, O., Ramyar, K., 2018. Effect of alkali activator concentration and curing condition on strength and microstructure of waste clay brick powder-based geopolymer. Compos. B Eng. 135, 242–252. https://doi.org/10.1016/j.compositesb.2017.10.013.

Ulugol, H., Gunal, M.F., Yaman, I.O., Yildirim, G., Sahmaran, M., 2021b. Effects of self-healing on the microstructure, transport, and electrical properties of 100% construction-and demolition-waste-based geopolymer composites. Cem. Concr. Compos. 121, 104081 https://doi.org/10.1016/j.cemconcomp.2021.104081.

Ulugol, H., Kul, A., Yildirim, G., Şahmaran, M., Aldemir, A., Figueira, D., Ashour, A., 2021a. Mechanical and microstructural characterization of geopolymers from assorted construction and demolition waste-based masonry and glass. J. Clean. Prod. 280, 124358 https://doi.org/10.1016/j.jclepro.2020.124358.

Verma, Y.K., Mazumdar, B., Ghosh, P., 2021. Thermal energy consumption and its conservation for a cement production unit. Environ. Eng. Res. 26 (3), 89–97. https://doi.org/10.4491/eer.2020.111.

Villagran-Zaccardi, Y.A., Marsh, A.T., Sosa, M.E., Zega, C.J., De Belie, N., Bernal, S.A., 2022. Complete re-utilization of waste concretes–Valorisation pathways and research needs. Resour. Conserv. Recycl. 177, 105955 https://doi.org/10.1016/j.resconrec.2021.105955.

Walkley, B., Provis, J.L., 2019. Solid-state nuclear magnetic resonance spectroscopy of cements. Mater. Today Adv. 1, 100007 https://doi.org/10.1016/j.mtadv.2019.100007.

Wallah, S., Rangan, B.V., 2006. Low-calcium Fly Ash-Based Geopolymer Concrete: Long-Term Properties. Faculty of Engineering, Curtin University of Technology, Perth (Australia).

Wan, Q., Rao, F., Song, S., Leon-Patino, C.A., 2017. Geothermal clay-based geopolymer binders: synthesis and microstructural characterization. Appl. Clay Sci. 146, 223–229. https://doi.org/10.1016/j.clay.2017.05.047.

Wu, H., Zuo, J., Yuan, H., Zillante, G., Wang, J., 2019. A review of performance assessment methods for construction and demolition waste management. Resour. Conserv. Recycl. 150, 104407 https://doi.org/10.1016/j.resconrec.2019.104407.

Xu, H., Van Deventer, J.S.J., 2000. The geopolymerisation of alumino-silicate minerals. Int. J. Miner. Process. 59 (3), 247–266. https://doi.org/10.1016/S0301-7516(99)00074-5.

Yildirim, G., Ashour, A., Ozcelikci, E., Gunal, M.F., Ozel, B.F., 2022. Development of geopolymer binders with mixed construction and demolition waste-based materials. Eng. Proc. 17 (1), 4. https://doi.org/10.3390/engproc2022017004.

Yildirim, G., Kul, A., Ozcelikci, E., Sahmaran, M., Aldemir, A., Figueira, D., Ashour, A., 2021. Development of alkali-activated binders from recycled mixed masonry-originated waste. J. Build. Eng. 33, 101690 https://doi.org/10.1016/j.jobe.2020.101690.

Yu, H., Yi, Y., Unluer, C., 2021. Heat of hydration, bleeding, viscosity, setting of Ca (OH)₂-GGBS and MgO-GGBS grouts. Construct. Build. Mater. 270, 121839 https://doi.org/10.1016/j.conbuildmat.2020.121839.

Zhang, B., Zhu, H., Feng, P., Zhang, P., 2022. A review on shrinkage-reducing methods and mechanisms of alkali-activated/geopolymer systems: effects of chemical additives. J. Build. Eng. 49, 104056 https://doi.org/10.1016/j.jobe.2022.104056.

Zhang, Z., Provis, J.L., Reid, A., Wang, H., 2014. Fly ash-based geopolymers: the relationship between composition, pore structure and efflorescence. Cement Concr. Res. 64, 30–41. https://doi.org/10.1016/j.cemconres.2014.06.004.

Zhou, S., Zhou, S., Zhang, J., Tan, X., Chen, D., 2020. Relationship between moisture transportation, efflorescence and structure degradation in fly ash/slag geopolymer. Materials 13 (23), 5550. https://doi.org/10.3390/ma13235550.

Zhu, X., Tang, D., Yang, K., Zhang, Z., Li, Q., Pan, Q., Yang, C., 2018. Effect of Ca(OH)₂ on shrinkage characteristics and microstructures of alkali-activated slag concrete. Construct. Build. Mater. 175, 467–482. https://doi.org/10.1016/j.conbuildmat.2018.04.180.